PARTIAL CORE BLOCKAGE SIMULATION USING COBRA-TF

A Thesis

by

CHRISTOPHER MICHAEL CHANCE

Submitted to the Office of Graduate and Professional Studies of
Texas A&M University
in partial fulfillment of the requirements for the degree of

MASTER OF SCIENCE

Chair of Committee,	Jean C. Ragusa
Co-Chair of Committee,	Yassin A. Hassan
Committee Member,	Hamn-Ching Chen
Head of Department,	Yassin A. Hassan

December 2014

Major Subject: Nuclear Engineering

ABSTRACT

COBRA-TF (CTF) was used to simulate the cooling capabilities for two reactor types that undergo different blockage scenarios. One case considered is a pool-type TRIGA reactor in which instrumentation tubes were inserted into existing coolant channels. The inclusion of the instrumentation tubes reduces the available coolant flow area, requiring an investigation of fuel coolability. The second case considered a pressurized water reactor (PWR) that has experienced a loss of coolant accident. Debris not stopped by the sump strainer can be deposited at the inlet of the core, creating blockage at the inlet of select assemblies. The blockage at the inlets could create a lack of cooling capability for the blocked assemblies and could result in fuel failure. CTF has not been widely used for testing these scenarios and the results should be compared alongside other simulations performed in STAR-CCM+ and RELAP5-3D.

For the TRIGA reactor simulations, limitations of CTF were discovered such as a lack of natural convection correlations and setbacks with transient simulations. Therefore, steady-state simulations were created based on input data from the Safety Analysis Report for the reactor and data obtained by STAR-CCM+ models of the core. Single pin analyses were conducted on 3 different fuel rods in order to determine if the fuel rods were at risk of overheating from the proposed modifications with the instrumentation tubes. Larger simulations that modeled two different 4x4 arrays of fuel rods within the TRIGA core were used to determine how well the coolant traversed through these areas with the instrumentation tubes inserted. The results for all

simulations were compared to STAR-CCM+ results from similar models and it was determined that the insertion of the instrumentation tubes in the TRIGA reactor would not be a concern for the safety of the reactor under normal operating conditions.

The PWR simulations revealed more limitations of CTF and did not prove fruitful in providing reliable results. The original goal was to employ CTF to model a PWR core in full detail in order to compare the results to a RELAP5-3D model that used a lumped approach. However, we encountered difficulties with CTF, mostly due to issues with transient simulations and parallel processing. Significant improvements were made to CTF over the course of this research and have resulted in a more robust and bug-free version of the code. However, CTF is still being developed and has some remaining hurdles to overcome before it can be used to reliably model the simulations that were planned. This research still continues today and CTF is being used and improved upon to become a more versatile sub-channel analysis code.

DEDICATION

I would like to dedicate this paper to my brother, Jason. You are my hero, and you will always be my strength to continue to pursue great ambitions. I love you.

ACKNOWLEDGEMENTS

I would like to thank my committee chair, Dr. Ragusa, for his guidance and support through the course of this research. His assistance level-headedness through the errors and chaos of using CTF have helped me stay confident that everything would work out. Thanks to my co-chair, Dr. Hassan, for assisting me and allowing me the opportunity to work with his students on these projects. Thanks to Dr. Chen for his support throughout this research and residing on my committee.

Special thanks also goes to a few of my fellow colleagues. Jan Vermaak, thank you for obtaining data from the Nuclear Science Center to be used in this research and for running the STAR-CCM+ simulations for the TRIGA reactor. Thank you also for your help arriving at conclusions on the phenomena that we observed with the TRIGA simulations. Rodolfo Vaghetto, thank you for allowing me to stop by your office often and ask questions regarding the RELAP5-3D simulations. I appreciate you explaining the RELAP5-3D models in detail when trying to find a best way to ultimately compare apples and oranges. Thanks to Lauren Garcia for allowing me to try and explain concepts from my research in a way that was easy for everyone to understand. I also appreciate your support throughout the course of my research, and for bringing me food and company during the late nights at my office.

I also want to extend my gratitude to the Institute of Nuclear Power Operations and the National Academy for Nuclear Training for their generous funding for me during the course of my research. Thanks to the Nuclear Energy University Program with the

U.S. Department of Energy for providing funding for the TRIGA research that took place. Thanks also goes to South Texas Project for allowing me the opportunity to simulate their reactors through funding provided to the Department of Nuclear Engineering at Texas A&M University.

Finally, thanks to my parents, Brad and JoAnne, for their encouragement, support, and love. You have molded me into the man I am today. Thank you for everything!

NOMENCLATURE

CFD	Computational Fluid Dynamics
COBRA-TF	Coolant-Boiling in Rod Arrays – Two Fluids
CTF	COBRA-TF (ORNL/CASL version)
GSI-191	Generic Safety Issue 191
LOCA	Loss-of-Coolant Accident
PWR	Pressurized Water Reactor
SAR	Safety Analysis Report
STP	South Texas Project
TAMU	Texas A&M University
TRIGA	Training, Research, Isotopes, General Atomics

TABLE OF CONTENTS

Page

Page

LIST OF FIGURES

FIGURE Page

FIGURE Page

LIST OF TABLES

1. INTRODUCTION

Generic Safety Issue 191 (GSI-191), "Assessment of Debris Accumulation on PWR Sump Performance," was a study to enhance the understanding of head-loss characteristics of the containment sump when calcium silicate insulation would accumulate on a Pressurized Water Reactor (PWR) sump screen during a Loss-Of-Coolant Accident (LOCA). It was postulated that during a LOCA, calcium silicate insulation on piping could be removed and degenerate into very fine particulates in the containment environment. This debris would then accumulate on a sump screen and cause substantial head loss across the sump screen. [1]

Another issue that developed from the investigation of GSI-191 concerned debris small enough that it could bypass the sump screen. If this debris were to travel to the core grid plate, it might collect on the grid plate and associated filter plate at the inlet of the core and block flow directly into specific assemblies. This could result in insufficient cooling of the core and ultimately lead to fuel failure.

The significance of this threat required an investigation of the capability of cooling the core with blocked flow into specific assemblies. Previous research conducted by Westinghouse found with 99.4% of the core inlet blocked, there could still be sufficient enough flow to remove the decay heat. [2] In this analysis, a three-loop downflow model plant rated for 2900 MW_{th} was chosen. Additionally, only 4 channels were modeled in this analysis: hot assembly channel, guide tube channel, non-guide tube channel, and low power periphery channel.

The Westinghouse investigation provided great insight to this issue. That being said, it may not accurately answer the issue for all reactor configurations. With this in mind, South Texas Project (STP) wanted an analysis performed that was representative of their Westinghouse four-loop PWR units. Working with Texas A&M University, a RELAP5-3D model was made of this scenario in order to include primary system data from RELAP5-3D to accurately model the situation as it progresses. [3] The RELAP5-3D model represents a lumped approach in that all sub-channels of each assembly are grouped together and are viewed as single channels through the core. Furthermore, RELAP5-3D is a system code, utilizing generic models in order to model multiple components of a plant. This results in assumptions and approximations to be made in order to model some components. [4] For example, in the RELAP5-3D model of the Westinghouse four-loop PWR unit, each assembly was modeled as a single pipe rather than a rectangular assembly. Furthermore, no sub-channels within each assembly were modeled. This made it desirable to model a similar scenario using a code with a specialized focus on the reactor core, such as a sub-channel analysis code, in order to determine whether the RELAP5-3D model was accurately depicting the situation within the reactor core.

With this in mind, Coolant-Boiling in Rod Arrays – Two Fluids (COBRA-TF) was for this project as it uses a two-fluid, three-field model rather than a two-field model that is common among other sub-channel codes. COBRA-TF also has the ability to simulate 3-dimensional configurations. [5] This is a desirable feature since the inlet to some assemblies will be blocked and phenomena such as counter-flow may be present

within the core. COBRA-TF was originally developed by Pacific Northwest Laboratory, but was continued by Pennsylvania State University and improved, updated, and re-branded as CTF. CTF considers liquid film, liquid droplets, and vapor as three separate fluid fields. Each field has its own set of conservation equations with one exception: it is assumed that the liquid and liquid droplet fields are in thermal equilibrium, therefore these two fields share the same energy equation. [5] The additional field of liquid droplets makes CTF an ideal code to use for modeling accident scenarios such as core blockages. With drastically reduced fluid flow through the core, the ability for a code to model this additional field may be helpful in determining the safety of the core and the system's ability to effectively transfer heat.

The other application of CTF investigated in this work pertains to the modeling of partial flow blockage in a research reactor. At Texas A&M University (TAMU), a Training, Research, Isotopes, General Atomics (TRIGA) pool type reactor is used for research and as a learning tool for students. TAMU received funding to perform multi-physics experiments with the TRIGA reactor in pulse mode in order to validate multi-physics codes. This would require high fidelity measurements in many locations within the TRIGA core that are currently available. In a proposed modification for the TRIGA reactor, more instrumentation in the form of neutron detectors and thermocouples could be inserted into tubes and placed in the existing coolant channels. Before this modification could be made, a safety analysis on the reactor must be performed to ensure that the modification will not harm the reactor or risk damage to the reactor due to reduced coolant flow in these channels. Both CTF and STAR-CCM+ were used to

model these modifications in order to determine whether safety limits could be maintained with the instrumentation tubes installed. The results for the two codes were compared and checked for agreement since empirical data cannot be obtained for the modified reactor.

The following sections will outline the work done on these two simulations. Section two will introduce the TRIGA reactor analysis in greater detail, followed by the results in section three. Section four will provide more information on the PWR analysis and will be followed with the findings in section five. Finally, section six will contain the conclusions that can be drawn from both projects as well as how well CTF performed throughout this research.

2. TRIGA REACTOR ANALYSIS

Texas A&M University (TAMU) received a grant to modify the TRIGA reactor in order to obtain a higher resolution of the neutron population within the core. This modification can then be used to improve multi-physics codes to increase their accuracy and help with verification and validation of the codes. The TAMU TRIGA reactor is slated to be modified to accommodate this detection system. The inclusion of this system would require instrumentation tubes housing neutron detectors to be inserted in the center of coolant channels throughout the core. These instrumentation tubes would effectively reduce the flow area of the channels in which they are inserted.

The TRIGA reactor has a unique and complex geometry as the grid plate permits a different inlet flow area for each coolant channel as it is currently designed. This results in a different inlet mass flow rate than in the bulk of the core. So, the proposed modification will not only change the flow area of each coolant channel, but will also change the inlet flow areas, thus affecting the inlet mass flow rate.

Due to these changes in the core geometry, primarily changes in the amount of coolant around the fuel rods, a sub-channel analysis of the TRIGA reactor was required to ensure that the modifications to the reactor would not introduce any risk of damage. The sub-channel analysis was carried out using COBRA-TF and was performed on localized areas within the reactor. Results of the CTF analysis were compared to a Computational Fluid Dynamics (CFD) analysis performed using STAR-CCM+ 8.06

using the shear-stress transport (SST) k-ω turbulence model on a 2 prism-layer mesh of the detector geometry. [6]

The TAMU TRIGA reactor is a 1 MWth pool type research reactor manufactured by General Atomics and uses natural convection to remove fission heat from the core. The core itself has an active fuel length of 0.381 m and comprises 90 large diameter fuel rods (3.5859 cm in diameter). The fuel rods are grouped in bundles of four rods each; in some bundles, a single fuel rod is replaced by either a fuel followed control rod (shim safety rods), a water followed control rod (regulating rod) or an air followed control rod (transient rod). During pulse operation, a pneumatic system can be used to eject the transient rod from the core nearly instantaneously, thus adding a large amount of positive reactivity to the core all at once. All of the bundles are located within a lower grid plate. Blocks of graphite for moderation and experiment tubes/locations are placed in the surrounding area of the core.

The entire core configuration can be seen in Figure 1. The grid for the reactor is a 6x9 in which each cell either contains graphite, instrumentation, a fuel bundle, or a location at which experiments can be inserted into the core. The white circles in Figure 1 are instrumentation within the core, be it either testing locations in which the pneumatic system are located or the reactor safety detectors located in column 1. The gold circle in Figure 1 is where the neutron source is located. The shim safety rods and regulating rod are fuel followed while the transient rod is gas followed in a guide tube.

The bundle locations are designated by a letter and a number as seen in Figure 1. For example, bundle D5 contains the transient rod. Within the bundles, a specific fuel

rod would be defined according to a directional quadrant relative to the center of the bundle. For example, the transient rod would be at the location D5SW, where D5 is the bundle location and SW is the South West rod location within that bundle. (NOTE: The north and south directions in Figure 1 are on the left and right sides of the figure, respectively.)

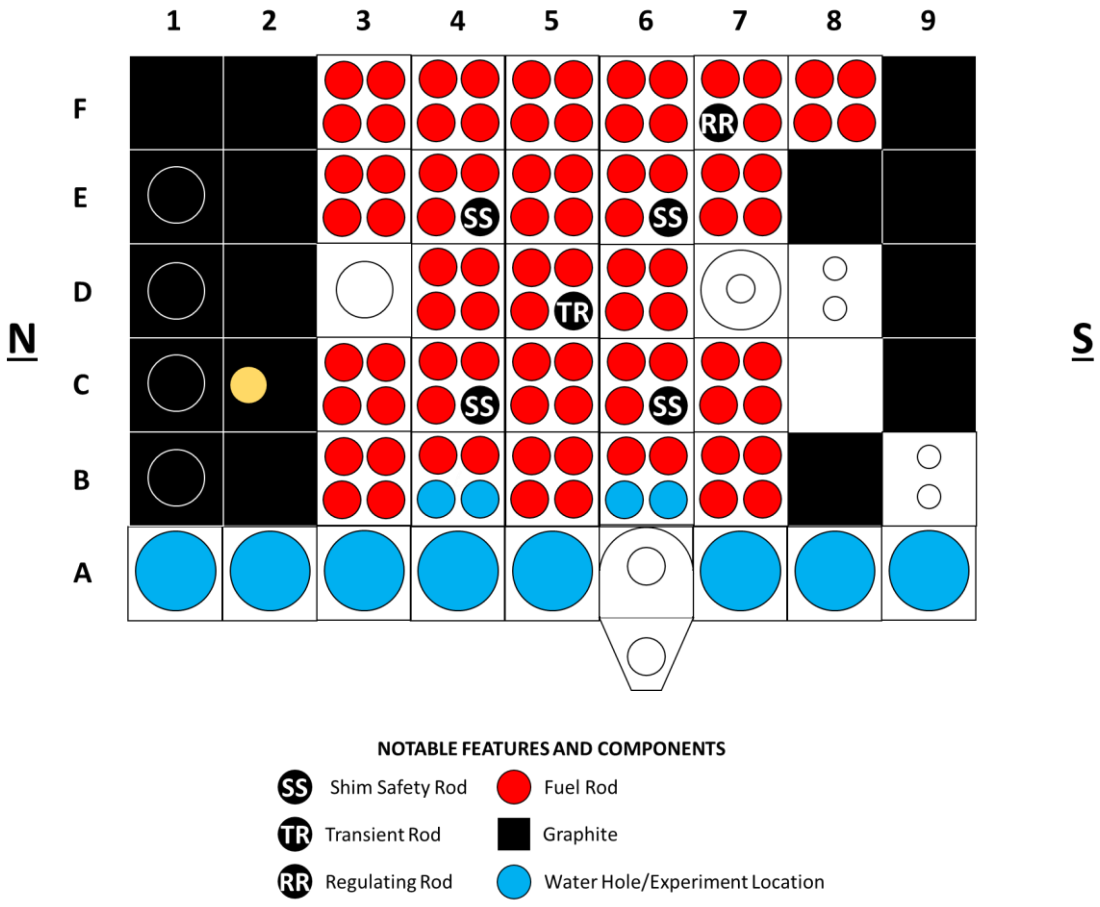

Figure 1. Layout of the TAMU TRIGA reactor core.

Due to a combination of the geometry and the hottest locations in the TRIGA core, it was decided that this analysis would only focus on two specific areas of the

TRIGA core, each containing a 2x2 array of four fuel bundles. These two areas are: the transient rod area (zone with the hottest rod in the core) and an area that contains only fuel. The "transient rod zone" contains bundles E4, E5, D4, and D5, and the "fuel-only zone" contains bundles F4, F5, E4, and E5. These two areas will be referred to as the *transient rod zone* and the *fuel-only zone* throughout the remainder of this document.

The TAMU TRIGA average rod power across the core is 11.11 kW/rod. Actual fuel rod total powers as well as axial power distributions were provided by the Nuclear Science Center staff at Texas A&M University. The transient rod zone has an average rod power of 12.46 kW and contains the highest power rod in the core (D5SE) at a power of 15.09 kW. The fuel-only zone being modeled has a local average rod power of 12.38 kW. The power rating of each rod in these two areas of interest can be seen in Figure 2, where the numbers in black are the power ratings for each rod and the numbers in red are the local rod number. It should be noted that in Figure 2, rod 14 in the left diagram and rod 6 in the right diagram are the same exact rod, which is a shim safety rod. Since the shim safety rods are fuel followed, these locations were modeled as if the rods were completely removed and the location was full of fuel.

Figure 2 also shows the cross sectional view at the inlet of the core. This view is different from a cross sectional view at the mid-plane of the core. This is because the core grid plate has holes drilled in it that only allow flow through at certain points. This is depicted in Figure 2 by the blue and black areas. The grey areas are where the core grid plate is a solid surface, therefore not allowing coolant to flow through. The only

way coolant can get to these areas at the bottom of the core is due to lateral flow either from surrounding channels or the periphery of the core.

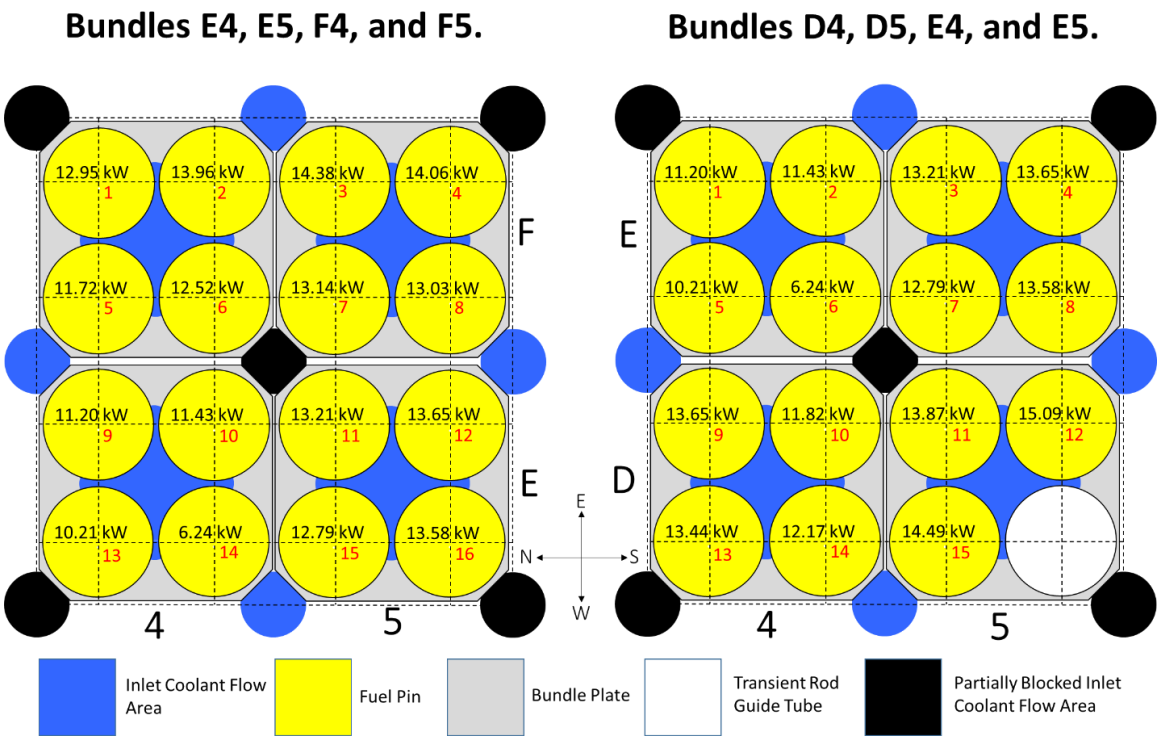

Figure 2. Depiction at the core inlet of where the instrumentation tube locations are creating partially blocked inlet coolant flow areas for specific channels, the power for each fuel rod, and sub-channel boundaries for both areas of interest.

The power distribution of the reactor was obtained from the Nuclear Science Center (NSC) staff. The total power for each rod was provided along with the relative power for each rod at 15 axial nodes. This data was used to provide CTF with the core radial power distribution as well as the axial power distribution for each rod.

Both models used the exact same geometry since the transient rod was modeled as a guide tube the same size of a fuel rod. The rod bundles are not actually spaced in a

perfect square, but rather a rectangle. In the north to south direction, the fuel pitch between two rods in adjacent bundles is 0.038227 m, and in the east to west direction, the fuel pitch between two rods in adjacent bundles is 0.0423672 m. A uniform square pitch was needed for CTF, so an approximated square pitch was made by taking the square root of the total area covered by four bundles and dividing by four, yielding a pitch of approximately 0.039566 m.

The instrumentation tubes will be inserted in every other channel location that lies between bundles. This spacing was chosen in order to try and allow as much flow as possible while still being able to obtain a high enough resolution for the spatial flux mapping in the core. Figure 2 shows the positions at which blocked coolant channels will be modeled, which are denoted by the black areas between and around fuel bundles.

Since the inlet flow area is not completely blocked for these channels, the new inlet flow area needed to be computed in order to determine the mass flow rate at the inlet for each channel. Figure 3 shows the sub-channels for the two areas of interest. In this diagram, the red number represents the local sub-channel number that lies within the dotted line box.

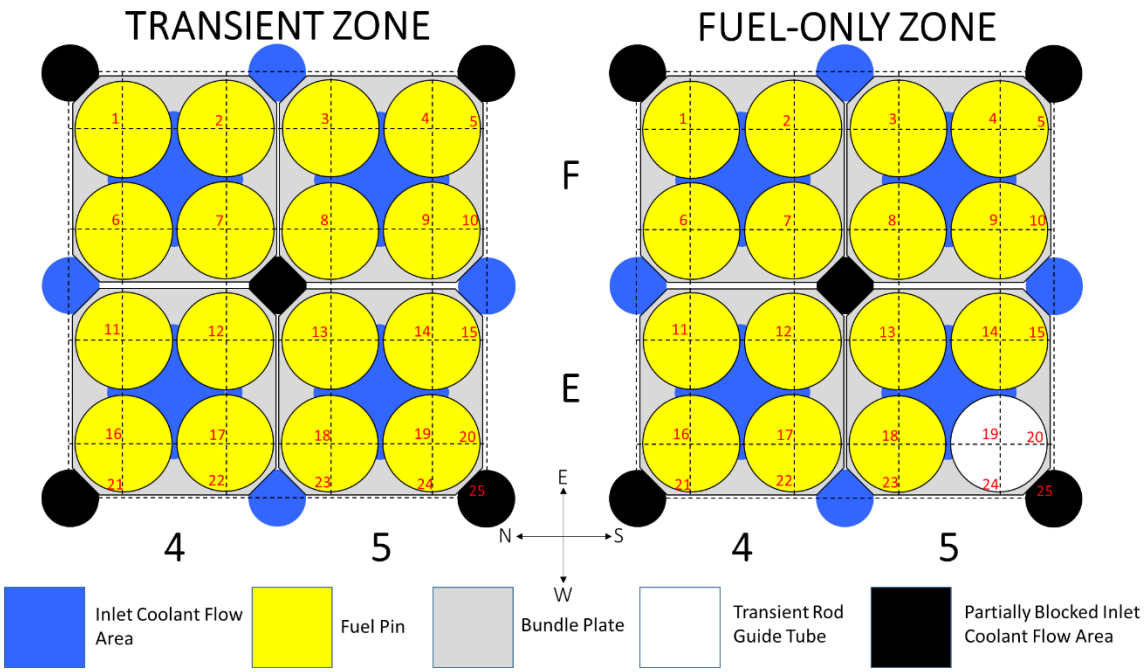

Figure 3. Sub-channel layout for the two models being investigated.

The inlet flow area (blue and black areas) varies from one sub-channel to another. The geometry for the TAMU TRIGA reactor was provided in order to determine the inlet flow areas for the existing configuration. Once altered, however, the inlet flow area for the blocked sub-channels would have to be computed. For the bulk of the blocked flow channels, the flow area is only reduced by the cross sectional area of the 1.27 cm diameter instrumentation tube that is being inserted along the length of the channel.

Since the inlet grid plate is designed in a way that limits the amount of flow into the bottom of the core, it is desirable to avoid reducing the amount of flow into the bottom of the core as much as possible. Figure 4 shows how the base of the

instrumentation tubes were designed in order to minimize the amount of blockage seen at the inlet grid plate. While the actual area of the channel will still be reduced, this design allows for maximum flow into the bottom of the core.

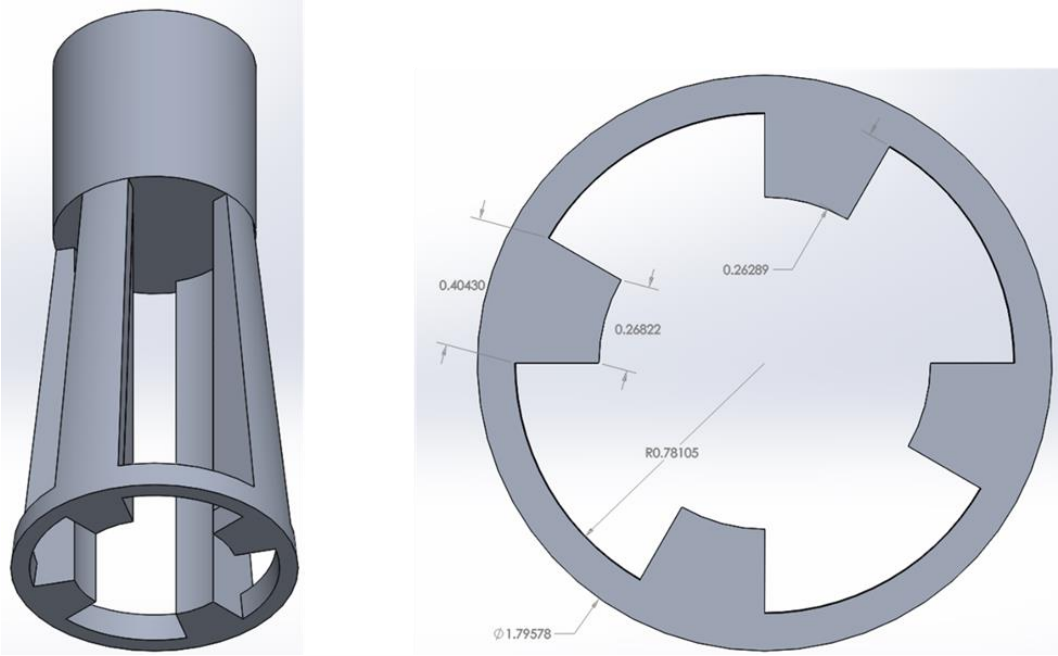

Figure 4. Conceptual design of the base of the instrumentation tube (dimensions are in centimeters).

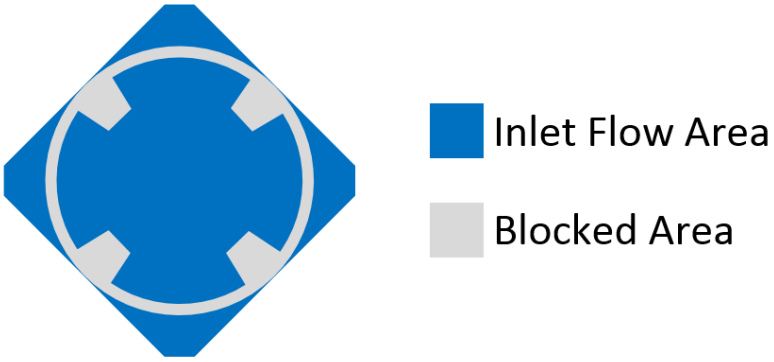

Figure 5. Sub-channel 13 inlet flow area as seen with the instrumentation tube inserted. (Not to scale.)

The inlet flow area for channel 13 would typically be a diamond-like shape whose dimensions are known. With the addition of the instrumentation tubes, the inlet flow area would appear as shown in Figure 5. The dimensions of the base of the instrumentation tube can be seen in Figure 4. The instrumentation housing will be a 1.27 cm diameter tube. In order to maximize flow while allowing support for the fission chamber, the guide tube will taper outward to a 1.79578 cm diameter tube and will rest upon the edges of the fuel bundle bases. The 1.79578 cm diameter tube will be hollow and have holes cut near the base as seen in Figure 4. The dimensions of the base of the instrumentation tube are as shown in Figure 4 as well.

Given these instrumentation tube base dimensions, the blocked inlet area was computed as a sum of the area covered by the outer ring and the area of the 4 fins that protrude inward. The area of each fin was approximated by the area of a trapezoid. The two bases of the trapezoid had lengths equivalent to the arc lengths at the inner and outer edges of the fins. This blocked area was only used at the inlet in order to assume a higher flow rate at the entrance into the core. The blocked area for the entire length of the core will be seen as a 1.27 cm diameter rod. This change in area at the inlet versus the bulk of the core will result in a change in the flow velocity through the core, i.e. the core inlet velocity will be higher than the core average velocity in this situation.

According to the TRIGA Safety Analysis Report (SAR), the average flow velocity through the core is 0.14 m/s. [7] In order to obtain this average core velocity, the mass flow rate for the model was determined using Equation 2.1.

$$\dot{m} = FA_{\text{model}} \rho_{inlet} \bar{v}_{core} \quad \text{(Eq. 2.1)}$$

where $\dot{m}$ is the mass flow rate (kg/s), FA_{model} is the flow area beyond the core inlet (m^2), ρ_{inlet} is the coolant density at the inlet (kg/m^3), and $\bar{v}_{core}$ is the coolant velocity through the core beyond the core grid plate (m/s). Equation 2.2 could then be used to determine the average inlet flow velocity:

$$\bar{v}_{inlet} = \frac{\dot{m}}{\rho_{inlet} FA_{core,inlet}} \quad \text{(Eq. 2.2)}$$

where $\bar{v}_{inlet}$ is the coolant velocity at the inlet (m/s), $FA_{core,inlet}$ is the flow area as seen at the core inlet in (m^2), and the other variables have been previously defined. Finally, the inlet mass flow rate for each channel was then determined using Equation 2.3.

$$\dot{m}_{chan,inlet} = FA_{chan,inlet} \bar{v}_{inlet} \rho_{inlet} \quad \text{(Eq. 2.3)}$$

where $\dot{m}_{chan,inlet}$ is the mass flow rate at the inlet for a particular channel (kg/s), $FA_{chan,inlet}$ is the flow area at the inlet for a particular channel in (m^2), and the other variables have been previously defined.

The inlet mass flow rate for each channel was computed in this manner in order to satisfy the average core velocity condition as well as the change in flow area between the inlet and the rest of the core.

Using the geometry and boundary conditions taken from the SAR, the CTF input decks were created pseudo-manually using the CTF preprocessor. The preprocessor was used to create the foundation of the CTF input decks using the known values from the

SAR. The preprocessor takes four input decks and uses them to create a single output that is used as the CTF input deck. The four input decks for the preprocessor include control.inp, which contains most of the simulation control parameters, geo.inp, which contains the parameters to map the core, power.inp, which contains power data for the simulation, and assembly.inp, which contains mostly geometry of the assembly for the simulation (this input deck has the capability of being renamed). Most parameters for the preprocessor input decks were left in the default settings such as the unit options, iteration convergence criteria, maximum number of iterations, Courant number, etc. Table 1 shows a general list of parameters that were used for most of the TRIGA simulations. Parameters such as number of fuel rods, total power, and mass flow rate varied depending on the simulation being run. However, the parameters contained within Table 1 and Table 2 remained mostly constant between all TRIGA simulations.

Table 1. control.inp and power.inp preprocessor input parameters for TRIGA

PARAMETER	INPUT DECK	VALUE	COMMENT
Rod Friction Factor Correlation	control	2	[8]
Entrainment and Deposition Model	control	0	Neither entrainment nor deposition
Mixing and Void Drift Model	control	0	Neither mixing nor void drift
Solver	control	0	Direct Gaussian
Initialization Rod Temp. (°C)	control	206.8	
Reference Pressure (bar)	control	1.8	Pressure at the top of the core
Reference Temp. (°C)	control	-30.0	Negative denotes temp. value
Reference enthalpy for noncondensables (kJ/kg)	control	303.464	[9]
Inlet Boundary Condition Type	control	2	Mass flow rate and enthalpy
Outlet Boundary Condition Type	control	1	Pressure and enthalpy
Inlet Temp. (°C)	control	-30.0	Negative denotes temp. value
Outlet Pressure (bar)	control	1.8	
Power Profile: Number of Pairs	power	15	Number of nodes for power profiles

Table 2. geo.inp and assembly.inp preprocessor input parameters for TRIGA

PARAMETER	INPUT DECK	VALUE	COMMENT
Number of fuel assemblies	geo	1	
Number of Fuel Assembly Types	geo	1	
Dimensions of Core Mesh	geo	1 1	only modeling "one" assembly
Symmetry Option	geo	1	
Fuel Assembly Map	geo	1 1	The first value is ignored (it is a place holder for organizing the input deck)
Number of Axial Groups	geo	14	
Active Length (mm)	assembly	381	Length of core
Conduction Model Flag	assembly	1	Radial conduction (See NOTE)
Fuel Pellet Diameter (mm)	assembly	34.823	
Radial Nodes in the Fuel Pellet	assembly	10	
Cladding Inner Diameter (mm)	assembly	34.829	
Cladding Outer Diameter (mm)	assembly	35.839	
Pin Pitch (mm)	assembly	39.56601	
Constant Gap Conductance (W/m^2K)	assembly	15764	
Cladding Material	assembly	SS304	
Number of Spacer Grids	assembly	0	
NOTE: Radial conduction was used alone. It was found in testing that when enabling both radial and axial conduction, there was no significant difference in results. Therefore, in order to reduce computational time, only radial conduction was activated.			

The power data can be seen in the Table A-1 as provided by the NSC staff. This data was used to create the axial power profiles across all simulations. The generated input decks were then manually altered by making edits to: the channel area and wetted perimeter in card 2.2, the material properties in card 10, the axial peaking map for each rod in cards 11.3 and 11.4, the power peaking factor for each rod in card 11.8, and the boundary conditions in card 13.4. Due to the nature of CTF, the inlet mass flow rate for

each channel was set individually in card 13.4 as an inlet boundary condition from values supplied by the STAR-CCM+ analysis. This was assumed to be acceptable since a steady-state simulation was being run and not a transient. Additionally, the average core velocity provided in the SAR was from a steady-state scenario. (Refer to Appendix B for examples of the input decks.)

The flow rates for each simulation varied and were dictated by the flow rates of the STAR-CCM+ simulation. Since the STAR-CCM+ simulations were based on natural convection, STAR-CCM+ did not have a user defined flow rate. Therefore, the mass flow rate was computed by STAR-CCM+ for each simulation. Since CTF requires a mass flow rate as an input, the STAR-CCM+ mass flow rates were used to create the input decks for CTF. Table 3 contains the mass flow rates used for the single pin simulations and Table 4 contains the mass flow rates used for the 4x4 rod simulations. Since a transient rod zone simulation was not made in STAR-CCM+, mass flow rate data was only obtained for the fuel-only zone. Therefore, the same flow rates were used in the transient rod zone as the fuel-only zone. While this is not realistic, it is hypothesized to be a good assumption. Since the transient rod zone has a very close average power rating compared to the fuel-only zone, it is assumed that the density of the coolant in these areas should be close to the same, therefore the buoyancy, the driving force of the flow, should be similar, creating similar mass flow rates since the geometry in these two areas are identical.

Table 3. Mass flow rates computed using STAR-CCM+ for single pin simulations.

ROD	BLOCKED/UNBLOCKED	MASS FLOW RATE (kg/s)
E5SW	Unblocked	0.0824
	Blocked	0.0808
C5SE	Unblocked	0.0828
	Blocked	0.0794
D4SW	Unblocked	0.0785
	Blocked	0.0755

Table 4. Mass flow rates used in the 4x4 pin simulations for both the transient rod zone and fuel-only zone.

Channel	Unblocked Mass Flow Rate (kg/s)	Blocked Mass Flow Rate (kg/s)
1	2.44142E-02	1.64396E-02
2	2.48728E-02	2.53298E-02
3	4.88284E-02	4.97255E-02
4	2.48728E-02	2.53298E-02
5	2.44142E-02	1.64396E-02
6	2.48728E-02	2.53298E-02
7	1.89102E-01	1.92576E-01
8	4.97456E-02	5.06596E-02
9	1.89102E-01	1.92576E-01
10	2.48728E-02	2.53298E-02
11	4.88284E-02	4.97255E-02
12	4.97456E-02	5.06596E-02
13	9.76568E-02	6.57584E-02
14	4.97456E-02	5.06596E-02
15	4.88284E-02	4.97255E-02
16	2.48728E-02	2.53298E-02
17	1.89102E-01	1.92576E-01
18	4.97456E-02	5.06596E-02
19	1.89102E-01	1.92576E-01
20	2.48728E-02	2.53298E-02
21	2.44142E-02	1.64396E-02
22	2.48728E-02	2.53298E-02
23	4.88284E-02	4.97255E-02
24	2.48728E-02	2.53298E-02
25	2.44142E-02	1.64396E-02
TOTAL	**1.545**	**1.506**

3. TRIGA REACTOR RESULTS

It was realized that COBRA-TF did not have natural convection correlations built into it. This resulted in forced convection correlations such as the Chen and Thom correlations to be used instead. While this doesn't affect the temperature of the coolant, it does result in incorrect fuel rod temperatures due to the incorrect calculation of the heat transfer coefficient. A STAR-CCM+ model of a single pin from the TRIGA reactor was created in order to run simulations to compare results with CTF. It was found that CTF and the STAR-CCM+ models had nearly identical axial temperature profiles for the coolant. However, CTF had lower fuel rod temperatures than STAR-CCM+ due to using forced convection correlations in CTF and natural convection correlations in STAR-CCM+. CTF is slated to be updated with natural convection coefficients eventually, however, for this research, it was decided to perform post processing on the output data in order to more accurately determine fuel rod temperatures.

Two preliminary models were created to compare results in order to make sure STAR-CCM+ and CTF agreed with each other in the most basic situations. Each model simulated 1 pin surrounded by coolant. The power for each pin was 11.11kW and had a flat axial power profile. The coolant had an inlet temperature of 30°C and the same mass flow rates of 0.074 kg/s for the unblocked models and 0.071 kg/s for the blocked models as determined by the STAR-CCM+ models. The STAR-CCM+ model was compared to empirical data to verify that the rod temperatures were accurate. This validated the STAR-CCM+ models, allowing the heat transfer coefficients to be

extracted and applied by hand to the CTF results. Using the CTF results for the coolant temperature profile in combination with the heat transfer coefficients supplied from STAR-CCM+, the fuel rod temperature profiles were determined analytically and agreed with the STAR-CCM+ model. Since the two codes agreed with each other for an elementary model, more detailed models relating directly to the TRIGA core were modeled next.

3.1 Single Pin Analysis and Comparison of STAR-CCM+ to CTF Analytical Model

The fuel rods that were modeled for comparison were C5SE, D4SW, and E5SW (see Figure 1). These fuel rods were simulated in STAR-CCM+ first in order to obtain the mass flow rate for each single channel. Once the mass flow rate was obtained, a similar model was created in CTF using this mass flow rate. The heat transfer coefficient from the STAR-CCM+ model was then used in post processing of the CTF data in order to compare STAR-CCM+ temperature profile results with the CTF based analytical temperature profile.

The power profiles for these three pins were provided by the Nuclear Science Center (NSC) staff and were used in both the CTF and STAR-CCM+ models. The total power for each rod is as follows: 13.58 kW for E5SW, 13.23 kW for C5SE, and 12.17 kW for D4SW. Figure 6 below shows the power profiles for each rod.

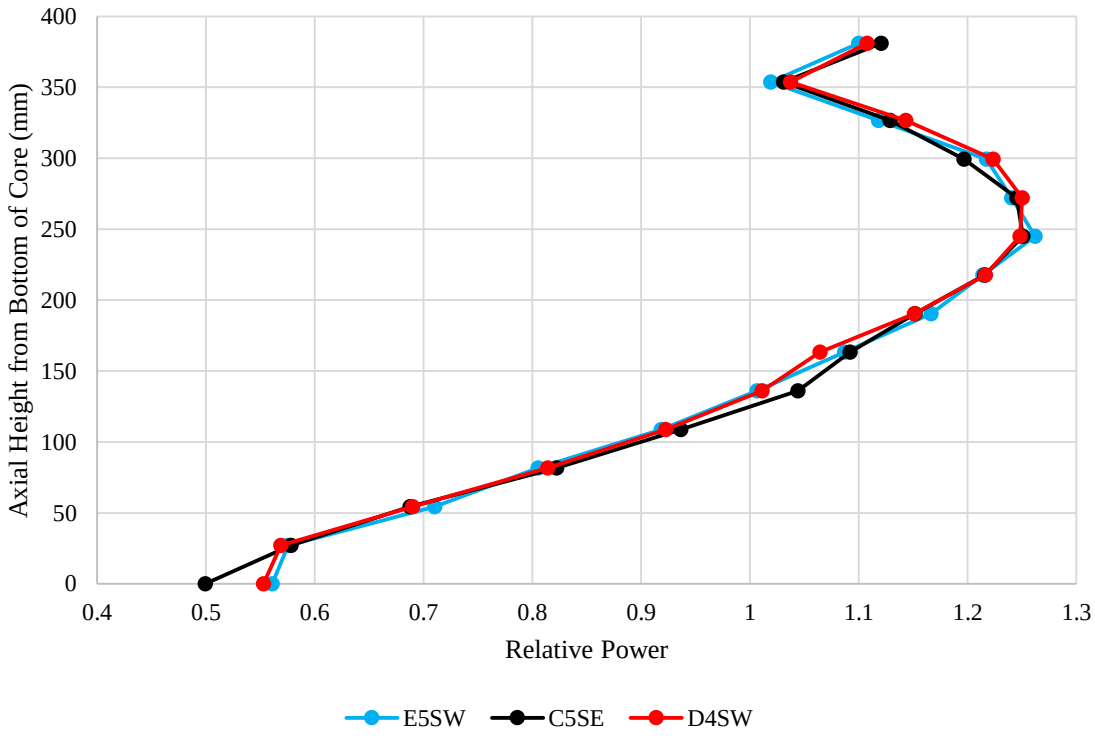

Figure 6. The power profile of the single fuel rods that were modeled for the CTF and STAR-CCM+ comparison.

Once the mass flow rate was found using STAR-CCM+, it was used to set the inlet boundary condition for CTF using the process described in section 2. The CTF model was then run to obtain a bulk coolant axial temperature profile, from which, the analytical model of the radial temperature profile could be determined. A diagram of the fuel rods in the TRIGA reactor is shown in Figure 7 to provide a visual of the regions within the fuel rods.

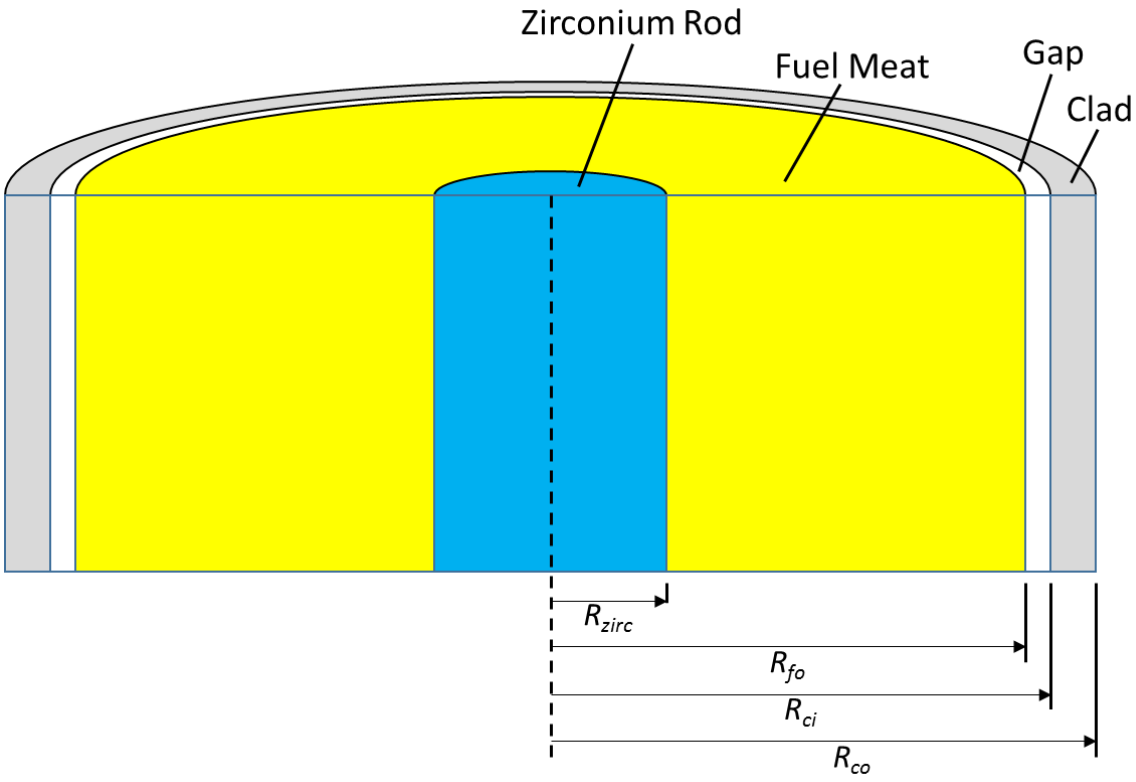

Figure 7. Diagram showing the regions of interest within the fuel rods of the TRIGA reactor (not to scale).

The analytical model used is based on the natural convection heat transfer coefficient that is determined by STAR-CCM+. It assumes conduction through the clad, gap, and fuel based on the thermal conductivity of the clad, conductance of the gap, and thermal conductivity of the fuel. Heat is only generated within the fuel meat as shown in Figure 7, therefore, conduction within the zirconium rod is not necessary for the model. Since CTF determines the bulk coolant temperature, and STAR-CCM+ uses a film temperature along the surface of the fuel rod, finding identical temperature profiles is not

expected, and it is anticipated that small discrepancies will be present. However, the change in temperature across each region (clad, gap, fuel) should be similar.

Using the known geometry of the fuel rods and the power profile, the linear power (kW/m) and volumetric heat generation (kW/m^3) were first determined for each axial node. Using the axial bulk coolant temperature profile from CTF and the heat transfer coefficient provided by STAR-CCM+, the outer clad temperature could be determined using Equation 2.4.

$$T_{co,j} = T_{bulk,j} + \frac{q'_j}{2\pi R_{co} h} \quad \text{(Eq. 2.4)}$$

where $T_{co,j}$ is the outer clad surface temperature (°C), $T_{bulk,j}$ is the bulk coolant temperate at axial node *j* (°C), q'_j is the linear heat flux at axial node *j* (kW/m), R_{co} is the radius of the outer surface of the clad (m), and *h* is the constant heat transfer coefficient (kW/m^{2}K) provided by STAR-CCM+.

From here, the conduction equation can be used to determine the inner clad temperature using the thermal conductivity of the clad using Equation 2.5.

$$T_{ci,j} = T_{co,j} + \frac{q'_j}{2\pi k_{clad}} \ln\left(\frac{R_{co}}{R_{ci}}\right) \quad \text{(Eq. 2.5)}$$

where $T_{ci,j}$ is the inner clad surface temperature (°C), k_{clad} is the thermal conductivity of the clad (kW/mK), R_{ci} is the radius of the inner surface of the clad (m), and $T_{co,j}$, q'_j, and R_{co} have all been previously defined.

The outer surface of the fuel temperature can then be determined by using the known conductance of the gap in Equation 2.6.

$$T_{fo,j} = T_{ci,j} + \frac{q'_j}{2\pi c_{gap} R_{gap}} \quad \text{(Eq. 2.6)}$$

where $T_{fo,j}$ is the outer fuel surface temperature (°C), c_{gap} is the conductance of the gap (kW/m^{2}K), R_{gap} is the radius of the gap located at the middle point between the fuel outer surface and the clad inner surface (m), and both $T_{ci,j}$ and q'_j have been previously defined.

Finally, the radial temperature profile through the fuel was derived from the steady-state heat conduction equation as seen in Equation 2.7. [10]

$$\frac{1}{r}\frac{d}{dr}\left(kr\frac{dT}{dr}\right) + q''' = 0 \quad \text{(Eq. 2.7)}$$

where r is the radius (m), k is the thermal conductivity (kW/m-K), T is the temperature (°C), and q''' is the volumetric heat flux (kW/m^3). The solution of this equation that was used in the CTF analytical model can be seen in Equation 2.8. The solution must be solved using radial nodes because unlike the other regions, heat generation will change depending on the radial location within the fuel. Equation 2.8 was used to determine the radial temperature profile up to the inner fuel surface using 11 radial nodes.

$$T_j(r) = T_{fo,j} + \frac{q'''_j}{2k_{fuel}}\left[\frac{1}{2}\left(R_{fo}^2 - r^2\right) - R_{zirc}^2 \ln\left(\frac{R_{fo}}{r}\right)\right] \quad \text{(Eq. 2.8)}$$

where $T_j(r)$ is the temperature of the fuel at axial node *j* and radius *r* (°C), $T_{fo,j}$ is the outer fuel surface temperature at axial node *j* (°C), q'''_j is the volumetric heat flux at axial node *j* (kW/m^3), k_{fuel} is the thermal conductivity of the fuel (kW/m-K), R_{fo} is the outer fuel radius (m), *r* is the radius of the fuel at which the temperature is desired (m), and R_{zirc} is the radius of the zirconium rod in the center of the fuel rod (m). Geometrical and material properties that were necessary for the creation of the analytical model can be found in Table 5. All geometric properties were found in the SAR. [7]

Table 5. Geometric and material properties for CTF analytical model.

PARAMETER	VALUE	COMMENT
Zirconium Rod Radius, R_{zinc} (m)	0.003175	
Fuel Diameter (m)	0.034823	
Gap Thickness (m)	0.000003	Compute R_{gap}
Clad ID (m)	0.034829	Compute R_{ci}
Clad OD (m)	0.035839	Compute R_{co}
Pitch (m)	0.038862	
Length (m)	0.381	
Thermal Conductivity of Fuel, k_{fuel} (kW/m-K)	0.018	[11]
Thermal Conductivity of Clad, k_{clad} (kW/m-K)	0.0162	[12]
Conductance of Gap, c_{gap} (kW/m^2-K)	15.764	Provided by NSC staff
Coolant Density (kg/m^3)	995.74	Value at inlet
Coolant Heat Capacity (kJ/kg-K)	4.18259	Value at inlet

When the combination of the geometry properties and the mass flow rate values, it can be seen that the velocity in these simulations is not 0.14 m/s as stated in the SAR. [7] However, due to the way STAR-CCM+ determined the mass flow rate and velocity based on natural convection, the CTF analytical models were created to match the

STAR-CCM+ model. Therefore, the STAR-CCM+ mass flow rates were still used, even if they corresponded to a velocity that was different than the SAR. This was done in order for the results from both codes to be compared.

Upon completion of the analytical model, the radial temperature profile at any axial node could be obtained and compared to the STAR-CCM+ results. This analysis was done for both unblocked and blocked single pin models. In the blocked single pin model, the flow area was reduced as if one of the proposed instrumentation tubes were inserted adjacent to the single fuel pin. This resulted in a different mass flow rate and heat transfer coefficient to be used in the CTF model. Figure 8 shows a comparison of the CTF and STAR-CCM+ radial temperature profile for the unblocked single pin analysis for rod E5SW.

As can be seen from Figure 8 (unblocked case) and Figure 9 (blocked case), the CTF Analytical model and the STAR-CCM+ agree on the radial temperature profile for rod E5SW. In these graphs, the maximum fuel temperature for the blocked case is actually lower than the unblocked case. This can be explained by three phenomena that are occurring. The obvious phenomena that would make one expect to see the fuel temperature increase in the blocked case is due to the constriction of flow. The effect of the flow constriction due to blockage resulted in less flow and resulted in an increase in the bulk coolant temperature from 49.51°C in the unblocked case to 54.52°C in the blocked case. This phenomenon has a positive feedback on the temperature of the fuel and should result in the fuel temperature increasing. For the second phenomenon, as the bulk fluid temperature increases, there is a change in buoyancy of the coolant which is

the driving force for the flow. This buoyancy change partially counters the effect of the constriction of flow, therefore has a negative feedback on the temperature of the fuel. For the final phenomenon, as the bulk coolant temperature increases, the natural convection heat transfer coefficient also increases. The heat transfer coefficient for the unblocked case in Figure 8 was 2574 W/m^{2}K while in the blocked case of Figure 9 it was 2713 W/m^{2}K. This increase in the heat transfer coefficient results in more efficient heat transfer from the fuel rod to the coolant. Therefore, it also has a negative feedback on the temperature of the fuel as it alone would also result in a lower fuel temperature.

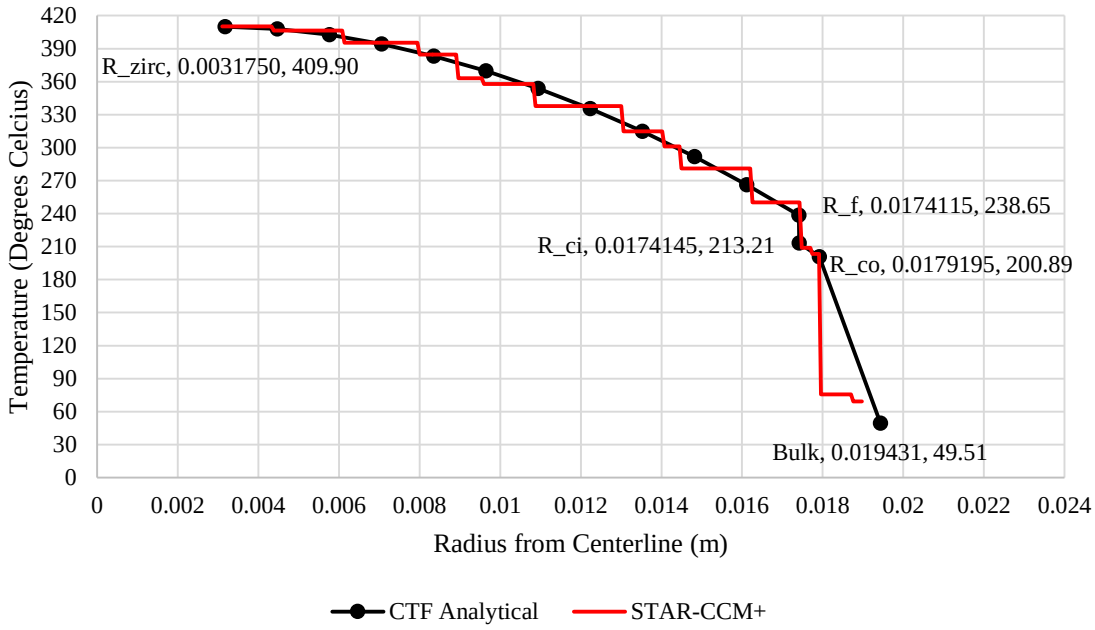

Figure 8. The comparison of STAR-CCM+ and CTF analytical unblocked radial temperature profiles for fuel rod E5SW at an axial height of 0.191 meters.

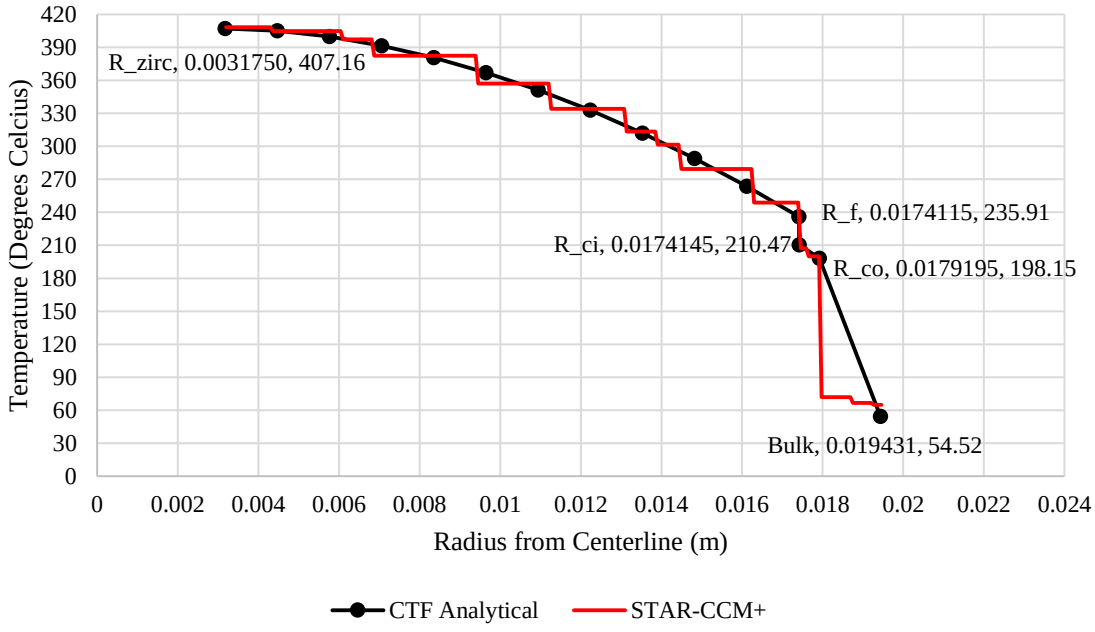

Figure 9. The comparison of STAR-CCM+ and CTF analytical blocked radial temperature profiles for fuel rod E5SW at an axial height of 0.191 meters.

Similar results can be seen for the two other single pin models that were run, C5SE and D4SW. In both of these rod simulations, there was a very strong agreement between STAR-CCM+ and CTF. The results for fuel rod C5SE can be seen in Figure A-1 (unblocked profile) and Figure A-2 (blocked profile) in Appendix A. The results for fuel rod D4SW can be seen in Figure A-3 (unblocked profile) and Figure A-4 (blocked profile) in Appendix A.

3.2 Fuel-Only Zone: Bundles E4, E5, F4, and F5

Once the single pin models were completed and showed agreement between STAR-CCM+ and CTF, more detailed models could be run. To keep things simple for STAR-CCM+, the fuel-only zone was modeled in both codes to compare results. The transient rod zone could be run in STAR-CCM+ as well, however, it is slightly more

complicated to develop. The fuel-only zone was designed for both models and successful runs were made from both codes. The summary of the results from CTF and its alignment with the STAR-CCM+ results are presented in this section.

The outlet temperature for each channel of the fuel-only zone in unblocked and blocked cases using CTF can be seen in Figure 10. Each sub-channel is shown using the dotted lines. The red numbers represent the local sub-channel number for each dotted line box. The black and white numbers represent the outlet temperature for each respective sub-channel that the value is contained within.

The maximum temperature of the hottest channel in the blocked case increased from 68.46°C in the unblocked case to 77.51°C in the blocked case as can be seen in channel 5 of Figure 10. The average temperature across this area increased from 58.71°C for the unblocked case to 59.72°C for the blocked case. With the boiling point at 116.9°C at this depth, even at the peak water temperature of 77.51°C, the water is almost 40°C sub-cooled.

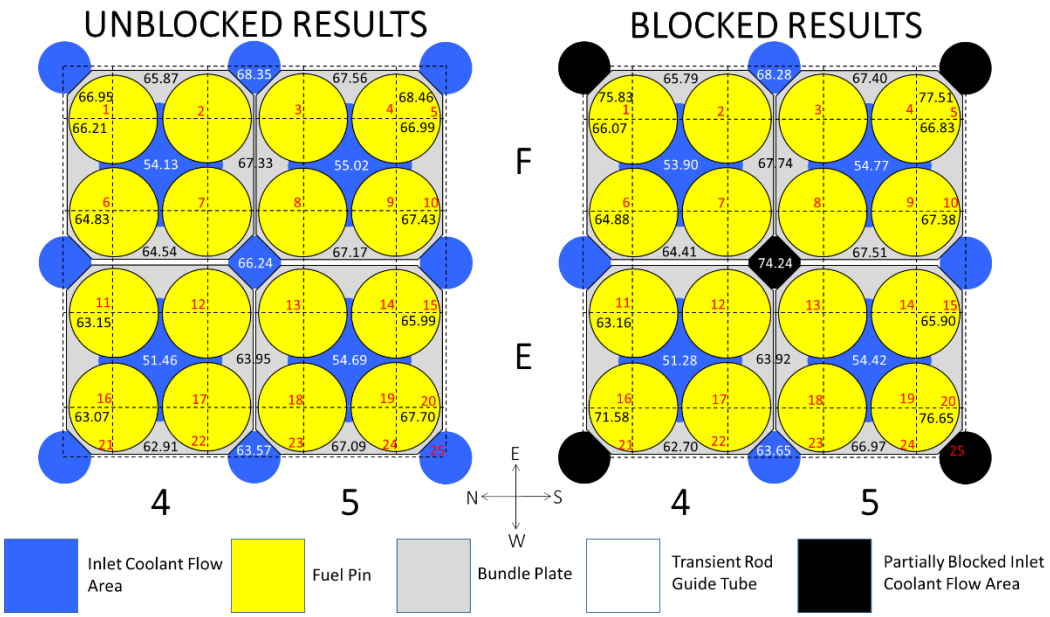

Figure 10. The sub-channel outlet temperatures using CTF for the fuel-only zone (unblocked model on the left and blocked model on the right).

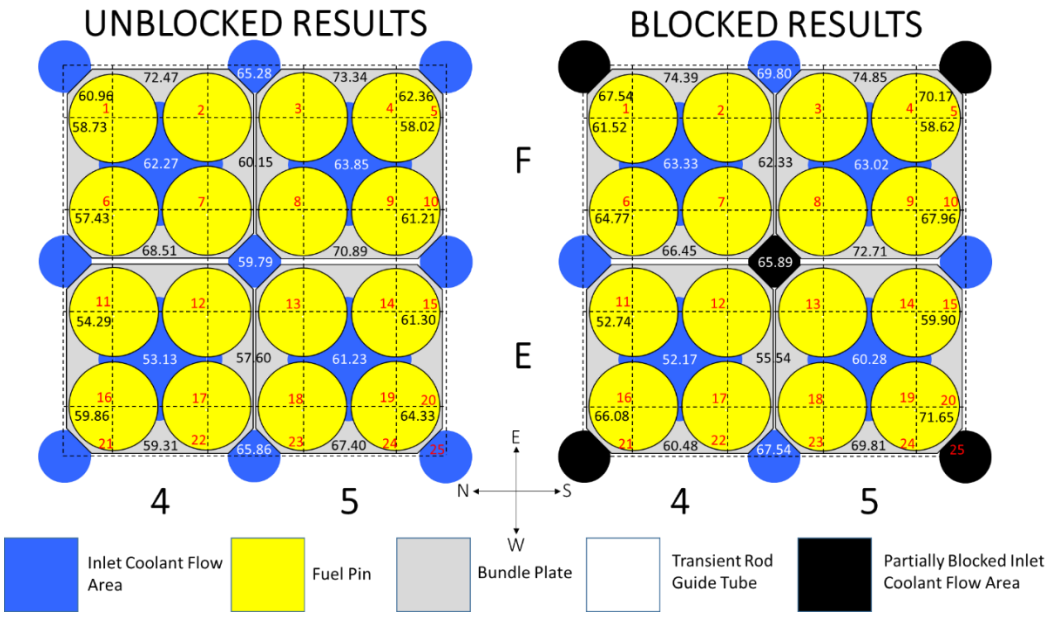

Figure 11. The sub-channel outlet temperatures for the fuel-only zone as determined by STAR-CCM+ (unblocked model on the left and blocked model on the right) [6].

Figure 11 shows the outlet temperatures according to the STAR-CCM+ model. The STAR-CCM+ results show the same trend as observed in the CTF results with an overall increase in average outlet temperate as well as blocked channels showing a significant increase in outlet temperatures. While the same trends are shown, there is clearly a difference in the resulting coolant temperature profiles between the two codes. This was not observed in the single pin simulations, but only the 4x4 rod simulation. The cause for this is unknown due to only having a single 4x4 rod simulation from STAR-CCM+ to compare. When more simulations can be compared between the two codes, a solution to this problem may be found. For now, some of the reasons for this disagreement could be due to the inherent differences between a sub-channel analysis code and a CFD code and how they each approach transverse flow. Furthermore, it could be due to the geometry differences in the two simulations. In STAR-CCM+, geometry above and below the active fuel line was modeled, whereas in the CTF simulation, all that was modeled was the full length of the active fuel. This could certainly create differences in how the fluid flows in both simulations. Another consideration is how thermodynamic properties of the coolant is determined. It has been determined that the way COBRA-TF determines thermo-physical properties is somewhat outdated and not consistent with the way they are determined in other codes that are currently being developed. [13] Lastly, this could be due to a user error in either the STAR-CCM+ or the CTF analysis. It took time in order to develop the single pin models so that both codes were modeling as similar situations as possible. The process of refining both simulations should be revisited for this larger scale model. While it will

certainly be time consuming for the STAR-CCM+ model, it is necessary to ensure that the models are modeling similar scenarios.

The fuel centerline and clad temperatures can be determined when the heat transfer coefficients can be determined by STAR-CCM+. Since the CTF analytical model is set up to use a single heat transfer coefficient for each rod, the STAR-CCM+ results will have to be parsed over and an average heat transfer coefficient will have to be determined for each rod. Once these heat transfer coefficients have been determined, the CTF analytical model can be used. Based on the analysis performed by the single pin models, this was not deemed an important issue for the analysis of the two four bundle zones that are being investigated. Since the analytical model is essentially measuring conduction through the fuel rods alone for a steady-state case, the CTF analytical model and STAR-CCM+ models should match exactly as they did in the single pin models. Therefore, assurance that the fuel and clad do not reach excessive temperatures according to the STAR-CCM+ model alone should be sufficient evidence to prove the safety of the modifications.

The surface temperature profiles from the STAR-CCM+ simulations can be seen in Figure 12. The color index displays temperatures ranging from 30^0C to 200^0C in order to allow the higher temperature zones to be seen with greater ease. The actual peak cladding temperatures were 276^0C for the unblocked case and 236^0C for the blocked case. [6] Once again, this observation may be counter-intuitive at first, but can be explained from the flow patterns seen in both STAR-CCM+ and CTF.

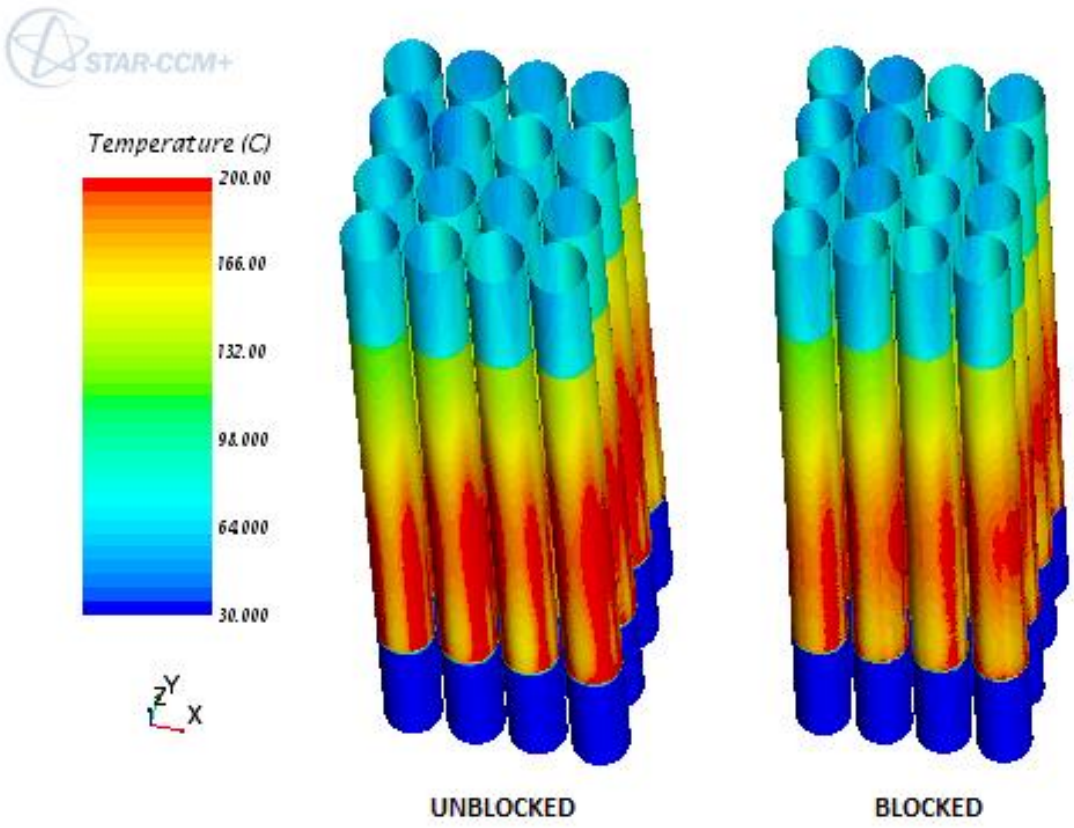

Figure 12. Surface temperature of fuel rods as determined by STAR-CCM+. [6]

In the STAR-CCM+ model, the flow within a sub-channel can be seen, whereas in CTF, only the flow between channels can be seen. That is, in CTF, the lateral flow through the "gaps" between each sub-channel is recorded and the actual flow within a sub-channel or within a particular axial node of a sub-channel cannot be seen. However, in the STAR-CCM+ simulation, the stream lines can be mapped within each sub-channel and within each axial node, not only at the interface between two sub-channels. The map of the streamlines show that the instrumentation tubes in the blocked case almost straighten the flow in that they allow the coolant to flow along the fuel rods rather than

flowing across the middle of a sub-channel. Without actually showing the movement of the streamlines, this can be discerned from Figure 13. The addition of the instrumentation tubes means that coolant can no longer flow through the middle of the channels, but must flow through the very edges of the channels and along the surface of the fuel rods. Therefore, the coolant is more efficient at removing heat from the fuel rods since it is forced to move along the rods rather than through the center of the sub-channel.

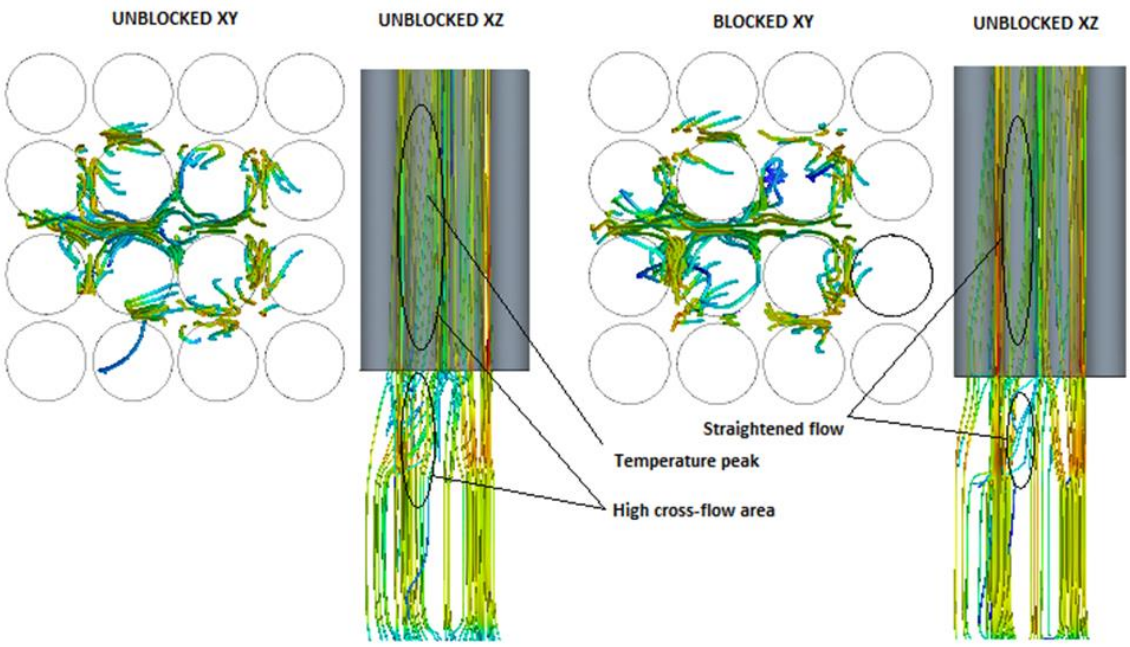

Figure 13. A plot of the streamlines at a particular instance of both the unblocked and blocked profiles for the fuel-only zone (generated by STAR-CCM+). [6]

In conjunction with the STAR-CCM+ results, the lateral flow results from CTF continue to explain the lower temperatures in the blocked case. The cross flow from

unblocked channels to blocked channels was expected to increase. Looking at the vertical mass flux for channel 5, a blocked channel, in Figure 14, it is noticeable that there is a significant increase in the change in flow between the unblocked and blocked cases. The mass flux was observed rather than the mass flow rate due to the change in flow area between the unblocked and blocked models. Therefore, the mass flux provides a better assessment of the increase of flow within a channel since the flow rate is divided by the flow area.

In channel 5 of the unblocked case, there was approximately a 20% increase in mass flux between the lowest point and the highest point in the flow profile. In the blocked case, the outlet flow was still lower than the unblocked case, however, there was a 52% increase in mass flux between the lowest point and the highest point. Even though there is a large blockage in the channel, the outlet mass flux is increased by over 11% from the unblocked case, while the mass flux just after the inlet was reduced by almost 14%. In order for this to happen, there must be a transfer of coolant from the surrounding channels via lateral cross flow.

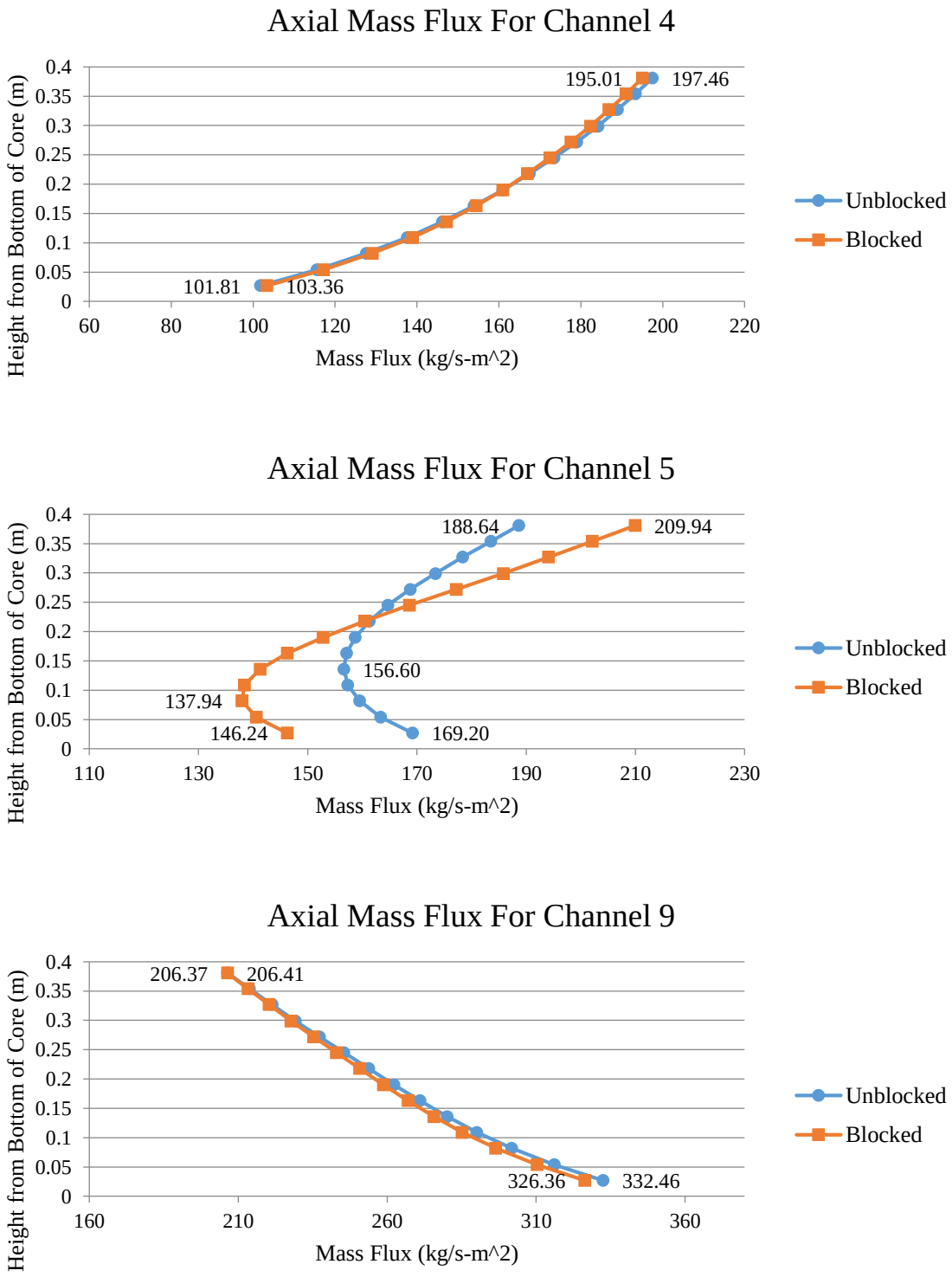

Figure 14. CTF vertical mass flux profiles for channels 4 (top), 5 (middle), and 9 (bottom) of the fuel-only zone for both the unblocked and blocked models.

While the transfer of coolant from the surrounding channels via lateral cross flow can be inferred from the axial mass flux of the surrounding channels, CTF provides the lateral mass flow rates for each channel. In CTF, each channel is separated by a non-physical boundary called a "gap." The gaps are defined by a width that is equivalent to the width between the two fuel rods that lie on each end of the gap as seen in Figure 15. In Figure 15, the gaps would be represented by the dotted lines. For coolant to flow from channel 1 to channel 2, it would have to pass through $Gap_{1,2}$. The amount of flow that moves through $Gap_{1,2,}$ would appear in the results of a CTF simulation. Using the CTF data for the lateral flow for all channels, the integral of the lateral flow along the entire length of the channels was taken and resulted in the data seen in Figure 16.

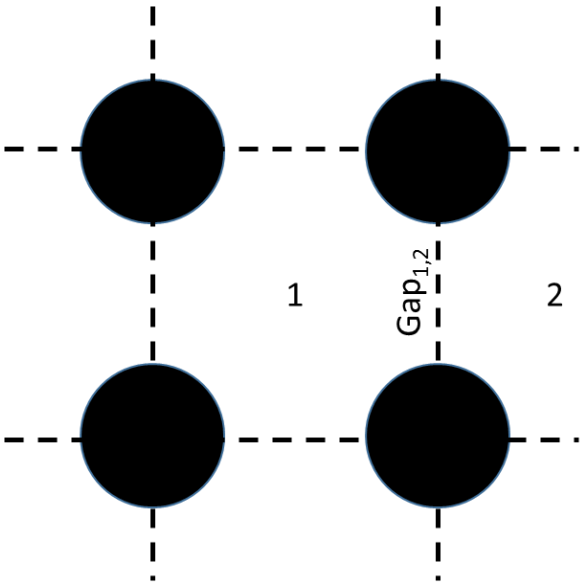

Figure 15. Depiction of the relations of gaps to sub-channel and fuel rod positions.

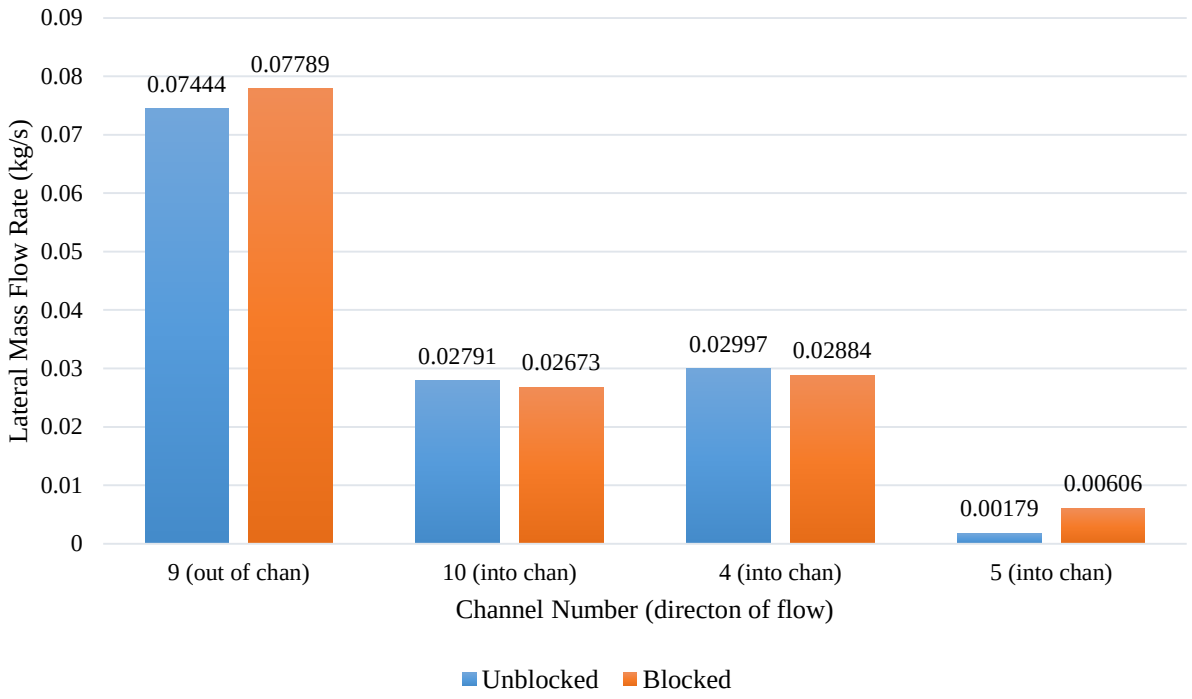

Figure 16. Comparison of integral lateral flow for channels 9, 10, 4, and 5 in the unblocked and blocked cases of the fuel-only zone (generated by CTF).

Channel 9, being one of the four channels in the model that have the highest inlet mass flow rates and surrounded by channels with much lower inlet mass flow rates, was expected to have a large lateral mass flow rate. This was verified the data as shown in Figure 16. Also as hypothesized, channels 10, 4, and 5 have net lateral mass flow rates into their respective channels. Most notable is the increase in lateral mass flow rate into channel 5 for the blocked case compared to the unblocked case. There was nearly a 240% increase in the lateral flow into channel 5 in the blocked case when compared to the unblocked case. While the lateral flow of channels 10 and 4 stayed nearly constant,

there was a nearly 5% increase in lateral flow out of channel 9 due to the blockage. A 5% increase results in an additional 0.00345 kg/s of flow being moved to other channels. In relation to channel 5, in the unblocked case, 0.00179 kg/s of flow were moving into channel 5, and in the blocked case, 0.00606 kg/s of flow were moving into channel 5, which is an increase of about 0.00427 kg/s. Since channels 10 and 4 are relatively unchanged in terms of lateral flow, most of the increase of the lateral flow from channel 9, if not all, is moving to the channels with blockage.

Furthermore, recall the findings from the single fuel pin models run in both STAR-CCM+ and CTF as seen in section 3.1. One of the findings showed that with an increase of coolant temperature, an increase in the heat transfer coefficient occurred. This correlation is also applicable in this larger model. Therefore, when the coolant in the blocked channels is increased, there is actually more efficient heat transfer taking place, thus reducing the temperature of the fuel rods. When the results from both STAR-CCM+ and CTF are combined, one realizes that while there is an increase in cross flow from one channel to another, the flow is forced to stay close to the fuel rods with the insertion of the instrumentation tubes. This results in the originally counter-intuitive peak cladding temperature results.

3.3 Transient Rod Zone: Bundles E4, E5, D4, and D5

The transient rod zone has still not been successfully modeled in STAR-CCM+ by the NSC staff. Once this zone has successfully been modeled, the results can once again be compared to CTF for validation. However, the transient rod zone has been successfully run in CTF, and the following results are presented below.

The outlet temperature for each channel of the transient rod zone in unblocked and blocked cases using CTF can be seen in Figure 17. Similar to Figure 10, each sub-channel is shown using the dotted lines, red numbers represent the local sub-channel number, and the black and white numbers represent the outlet temperature for each respective sub-channel.

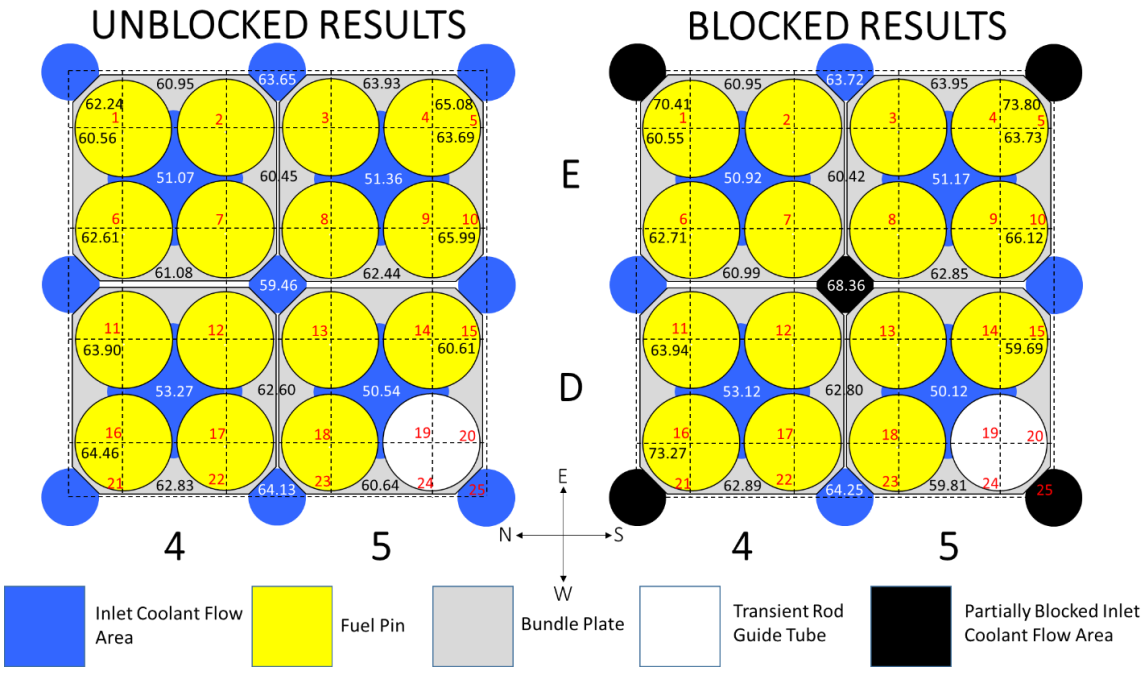

Figure 17. The sub-channel outlet temperatures using CTF for the transient rod zone (unblocked model on the left and blocked model on the right).

The maximum temperature of the hottest channel increased from 65.08°C in the unblocked case to 73.80°C in the blocked case as can be seen in channel 5 of Figure 17. The average temperature across this area increased from 57.53°C for the unblocked case to 58.21°C for the blocked case. With the boiling point at 116.9°C at this depth, even at the peak water temperature of 73.80°C, the water is over 40°C sub-cooled.

The cross flow was expected to increase in the blocked channels. Looking at the vertical mass flux for channel 5 in Figure 18, it is noticeable that there is a significant increase in the change in flow between the unblocked and blocked cases. The mass flux was observed rather than the mass flow rate due to the change in flow area between the unblocked and blocked models. Therefore, the mass flux provides a better understanding of the increase of flow within a channel since the flow rate is divided by the flow area.

In the unblocked case, there was about a 22% increase in mass flux between the lowest point and the highest point in the flow profile. In the blocked case, the outlet flow was still lower than the unblocked case, however, there was a 50% increase in the mass flux between the lowest point and the highest point. Even though there is a large blockage in the channel, the outlet mass flux is increased by almost 8% from the unblocked case, while the mass flux just after the inlet was reduced by almost 13%. In order for this to happen, there must be a transfer of coolant from the surrounding channels via lateral cross flow.

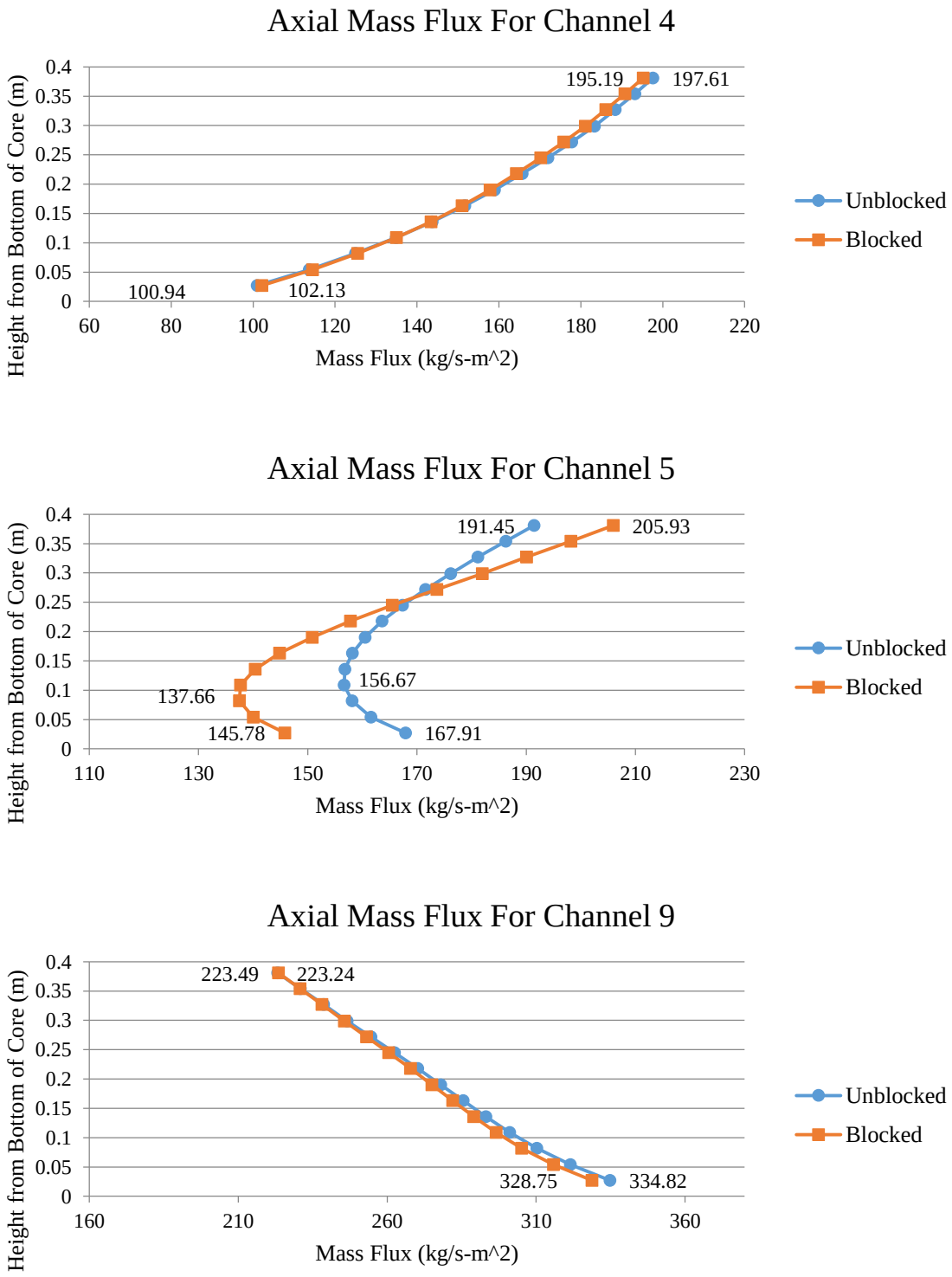

Figure 18. CTF vertical mass flux profiles for channels 4 (top), 5 (middle), and 9 (bottom) of the transient rod zone for both the unblocked and blocked models.

While the transfer of coolant from the surrounding channels via lateral cross flow can be inferred from the axial mass flux of the surrounding channels, CTF provides the lateral mass flow rates for each channel. Using the CTF data for the lateral flow for all channels, the integral of the lateral flow along the entire length of the channels was taken and resulted in the data seen in Figure 19.

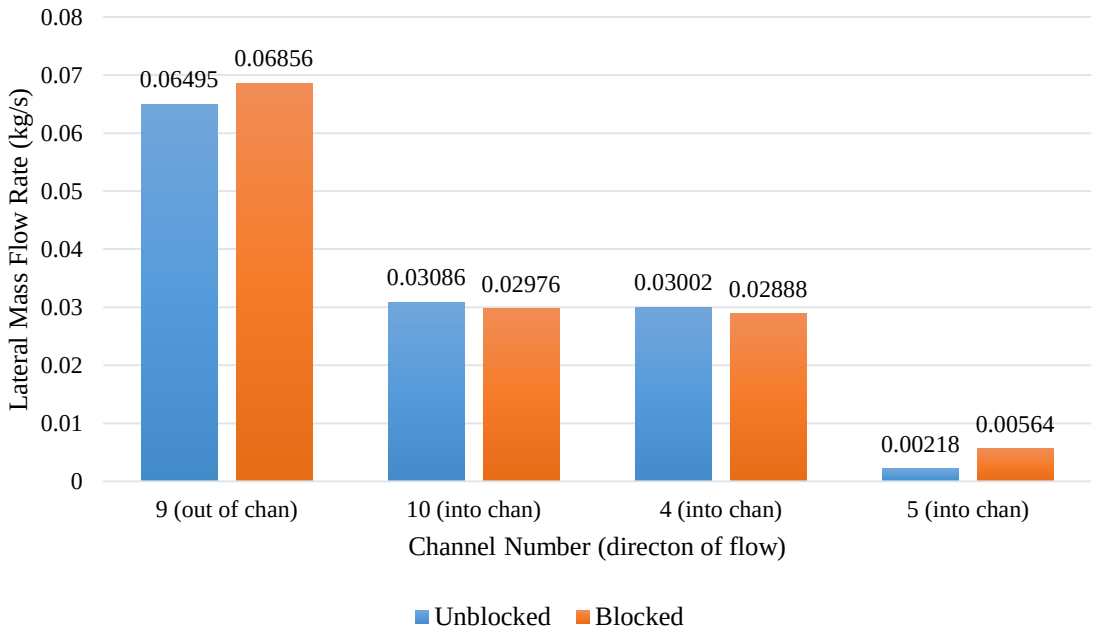

Figure 19. Comparison of integral lateral flow for channels 9, 10, 4, and 5 in the unblocked and blocked cases of the transient rod zone (generated by CTF).

The results in Figure 19 are very similar to the results found in the fuel-only zone. Channel 9, being one of the four channels in the model that have the highest inlet mass flow rates and surrounded by channels with much lower inlet mass flow rates, was hypothesized to have a large lateral mass flow rate out of channel 9. This was verified

by this data as shown in Figure 19. Also as hypothesized, channels 10, 4, and 5 have net lateral mass flow rates into their respective channels. There was nearly a 160% increase in the lateral flow into channel 5 in the blocked case when compared to the unblocked case. While the lateral flow of channels 10 and 4 stayed nearly constant, there was a nearly 5% increase in lateral flow out of channel 9 due to the blockage. A 5% increase for channel 9 results in an additional 0.00361 kg/s of flow being moved to other channels. In relation to channel 5, in the unblocked case, 0.00218 kg/s of flow were moving into channel 5, and in the blocked case, 0.00564 kg/s of flow were moving into channel 5, which is an increase of about 0.00346 kg/s. So it can be seen that since channels 10 and 4 are relatively unchanged in terms of lateral flow, most of the increase of the lateral flow from channel 9, if not all, is moving into the channels with blockage.

4. PRESSURIZED WATER REACTOR ANALYSIS

A study of GSI-191 conducted employed RELAP5-3D to simulate blockage at the inlet of all assemblies except for one in the South Texas Project reactor core. In the RELAP5-3D simulation the sub-channels of all 193 fuel assemblies are not modeled. Rather, all of the sub-channels from a single assembly are lumped into a single pipe geometry in RELAP5-3D. This lumped approach leads to problems that can be run much faster than modeling in full detail and use less computing resources. However, using RELAP5-3D in this manner is outside the typical use of the code package and it was desirable to compare RELAP5-3D's use for this analysis to a code that is designed for sub-channel analysis. With this in mind, CTF was used for this project as it uses a two-phase, three-field model rather than a two-field model that many other codes implement.

The model was built to represent the Westinghouse four-loop reactor used at South Texas Project. This particular reactor core contains 193 17x17 fuel assemblies, each assembly being 14ft long. For CTF to run in parallel, the code requires one processor per assembly being modeled. Therefore, a full core simulation would require 193 processors. This was not an option due to a lack of computational resources, therefore, smaller simulations only showing part of the core would be investigated.

The assembly and fuel parameters such as geometry, power, and flow rates are known for the Westinghouse four-loop reactor. While the RELAP5-3D model does not take these parameters into consideration due to the coarse lumping method and inherent

nature as a system code, CTF will require it with the level of detail that is desirable for this analysis. Figure 20 shows the layout of the fuel assemblies that are used in the reactor model being simulated. Table 6 shows the values for common geometry and flow values that are necessary to set up the CTF input decks.

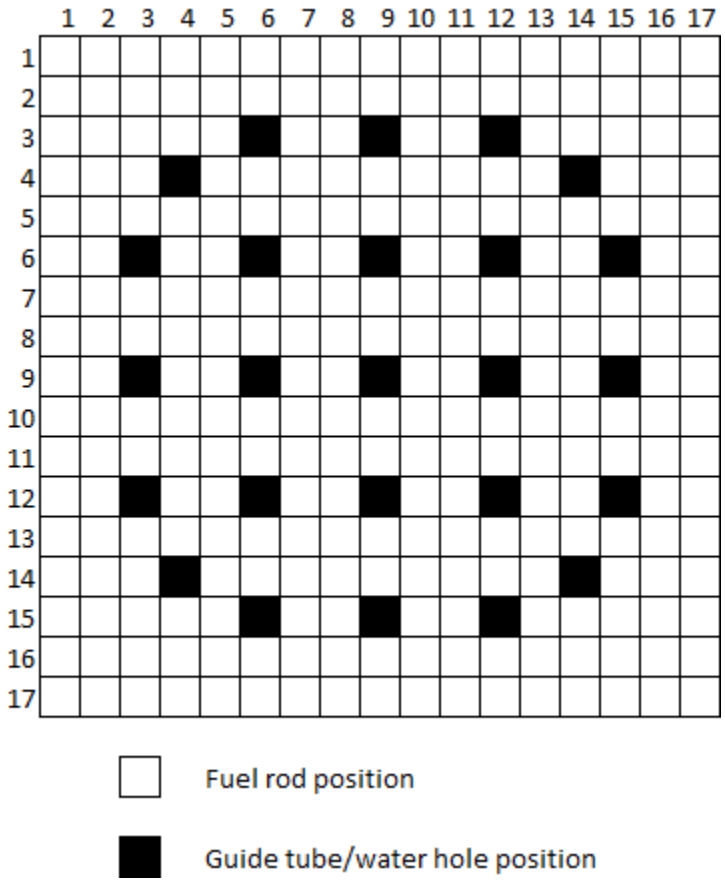

Figure 20. Layout of a 17x17 fuel assembly that is used in the Westinghouse four-loop reactor.

Table 6. Important parameters pertaining to the Westinghouse four-loop PWR reactor model.

PARAMETER	VALUE	COMMENT
Number of Assemblies	193	
Fuel Rods per Assembly	264	
Number of Fuel Rods in Core	50,952	
Total Core Power (MWth)	3819	
Nominal System Pressure (bar)	155.13	[14]
Nominal Inlet Temp (°C)	294	[14]
Fuel Pitch (mm)	12.5984	[15]
Fuel Rod Diameter (mm)	9.4996	[15]
Clad Thickness (mm)	0.5715	[15]
Gap Thickness (mm)	0.1651	[15]
Fuel Pellet Diameter (mm)	8.1915	[15]
Fuel Height (m)	4.2672	[15]
Guide Tube OD (mm)	12.2602	[16]
Guide Tube ID (mm)	11.4588	[16]

The RELAP5-3D model was run as a transient simulation in which the mass flow rate changes as a function of time. CTF was originally planned to be run in the same manner, however, with further use of CTF it was discovered that the mass flow rate in CTF could not currently be changed over the course of the simulation. As a work around to this issue, CTF would be used to run steady-state simulations at specific times along the transient where the mass flow rate was recorded from the RELAP5-3D simulation. In order to attempt to compare the results from both CTF and RELAP5-3D, the mass flow rates that were used in CTF were obtained from RELAP5-3D.

Lastly, the axial power profile for the PWR model was obtained from Westinghouse as proprietary information and utilized in the RELAP5-3D simulations. The exact same axial profile was used in CTF. Since the RELAP5-3D model utilized

such a coarse lumping scheme, a radial power profile for each assembly was not required. Since CTF would need this information though, a radial power profile for a 17x17 Westinghouse PWR assembly was obtained from an example provided in the CTF code package.

The input decks were generated similarly to the way they were for the TRIGA simulations. The preprocessor tool was used to create the CTF input decks to be used, and the CTF input decks were then cross-checked manually.

While preliminary work was done for this project and appeared to be very promising early on, it was later learned that CTF was plagued with bugs and limitations that were not realized early on. This project ultimately was fruitful in making significant advancements to the CTF code, however, has yet to yield a code that can sufficiently perform the analysis that is needed. The findings of this project are described in the remainder of this chapter. The findings include bugs that were found with the code, improvements made to the code, and limitations that were discovered that are inherent to the code's design that were not seen early on and may affect the way this analysis can be addressed in the future.

5. PRESSURIZED WATER REACTOR RESULTS

The PWR analysis was originally started before the TRIGA analysis. At the time, preliminary testing of CTF began to determine if CTF would be able to perform blockage simulations. This was done by creating very basic simulations in CTF that could be checked by hand. The preliminary studies held great hope for CTF to be used in larger and more complex simulations. However, upon further use of CTF, there were many limitations of CTF that were discovered and slowed the progress on the PWR analysis.

5.1 Preliminary PWR Analysis

Before the issues discovered in CTF stalled this endeavor, a small blockage simulation was run with CTF to determine the adequate approach to model blockage in a larger core. In this simulation, four PWR 17x17 assemblies were arranged in a 2x2 lattice. In the unblocked case, all assemblies received full inlet flow; in the blocked case, three of the assemblies were blocked at the inlet and only one was open as seen in Figure 21.

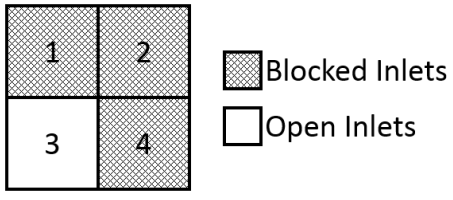

Figure 21. Configuration for the preliminary PWR blocked simulation.

The power was set to 7.2% of the full power to represent the amount of decay power approximately 1 second after the reactor has been scrammed from full power operation. Both a blocked and unblocked situation were run in order to compare the results. The reliability of CTF was checked by comparing the outlet temperatures from the results to the outlet enthalpy value at steady-state as given by Equation 5.1,

$$h_{out} = h_{in} + \frac{\dot{Q}}{\dot{m}} \qquad \text{(Eq. 5.1)}$$

where h_{out} is the outlet coolant enthalpy, h_{in} is the inlet coolant enthalpy, $\dot{Q}$ is the total power of the four fuel assemblies, and $\dot{m}$ is the mass flow rate through the four assemblies. Each of these parameters was taken from the CTF output except for the outlet enthalpy, which can be solved for. For the unblocked case, the inlet enthalpy was set to 1282 kJ/kg based on industry standards for a PWR at a nominal pressure of 155.13 bar and inlet coolant temperature of about 290°C, the total energy input was 5698.8 kJ/s based on 7.2% of full power for the 3819 MWth reactor being modeled. The mass flow rates were to be supplied by the RELAP5-3D model. However, a four assembly model had not been tested in RELAP5-3D, therefore accurate mass flow rates could not be acquired for this simulation. Therefore, the mass flow rates were estimated based on industry standards and a mass flux of 4197.198 kg/(s-m^2) was used in CTF. This correlated in the CTF output showing a mass flow rate of 511.81 kg/s based on the geometry used in the model. By Equation 5.1, the outlet enthalpy for this simulation should be about 1293 kJ/kg. Upon completion of this simulation, the outlet enthalpy

was computed by CTF to be about 1296.4 kJ/kg, deviating from the theoretical value by 0.26%.

Since the blocked simulation was also a steady-state simulation, energy conservation could be checked for it as well. In CTF, it was seen that the flow for each assembly could be controlled using a single mass flux defined in card group 1 of the individual assembly input decks for a parallel simulation. Using this method, the flow was restricted into assemblies 1, 2, and 4 by setting the inlet mass flux to the very small value of 0.0000001 kg/(s-m^2). The open assembly, assembly 3, retained the same inlet mass flux of 4197.198 kg/(s-m^2) that was used in the unblocked case. The total inlet mass flow rate for this simulation was 127.86 kg/s. This was later determined to be a very conservative estimation because in a real world situation, some of the flow from the nearby blocked assemblies would be redirected through the open assembly. The total energy input and inlet enthalpy were unchanged in the blocked simulation. Equation 5.1 suggests that the average outlet enthalpy for the core should be about 1327 kJ/kg. The average outlet enthalpy computed by CTF was about 1339 kJ/kg, deviating from the theoretical value by 0.9%.

The deviation of the CTF results from these two simulation from the theoretical values did create some concern. This led to an investigation of the thermodynamic property tables that are used with CTF. It is believed that the tables that are used in CTF may not agree with industry standards that are used today. In another study of CTF, it was determined that the thermo-physical properties within CTF are a bit outdated and

may not agree with what is currently used in other codes as well as what is generally accepted across the industry today. [13]

In the blocked simulation, it was assumed that the cross flow within the model would be significant enough that the flow rate at the outlet of each assembly should not have much variance. Furthermore, we should also note using the blocked simulation that whether the decay heat can appropriately be removed, and thus the outlet coolant should not reach the boiling temperature.

This analysis made it believable that channels could be successfully modeled as blocked by controlling the inlet mass flow rate. Looking at the mass flow rate for the channels in each assembly, it is conclusive that there was in fact a significant difference in the mass flow rate at the first node of the blocked assemblies compared to the open assembly. At the outlet, the mass flow rate was relatively constant across all four assemblies. Assembly 1 had and outlet mass flow rate of 33.74 kg/s, assembly 2 had 32.33 kg/s, assembly 3 had 31.78 kg/s, and assembly 4 had 30.35 kg/s. This confirms that there was significant cross flow within the core.

In viewing the visualization files that were produced by CTF, at the inlet, it is clear that the enthalpy was the lowest in assembly 3 where the majority of the coolant was entering since assemblies 1, 2, and 4 were blocked, as seen in the left plot of Figure 22. At the outlet, as seen in the right plot of Figure 22, while there is still a definite gradient in enthalpy, the distribution across the model is much more homogenized than at the inlet. The highest enthalpy in the model was 1401.4 kJ/kg as found in channel 19 of assembly 2 (top right corner of the outlet enthalpy plot of Figure 22). However, it

was later realized that this is not a good representation of what could actually be expected. This simulation was run at steady-state using a nominal system pressure. During the accident scenario that was conducted using RELAP5-3D, the pressure would be expected to drop as low as 2 bar. Therefore, this preliminary simulation cannot accurately determine if the coolant will actually avoid boiling conditions.

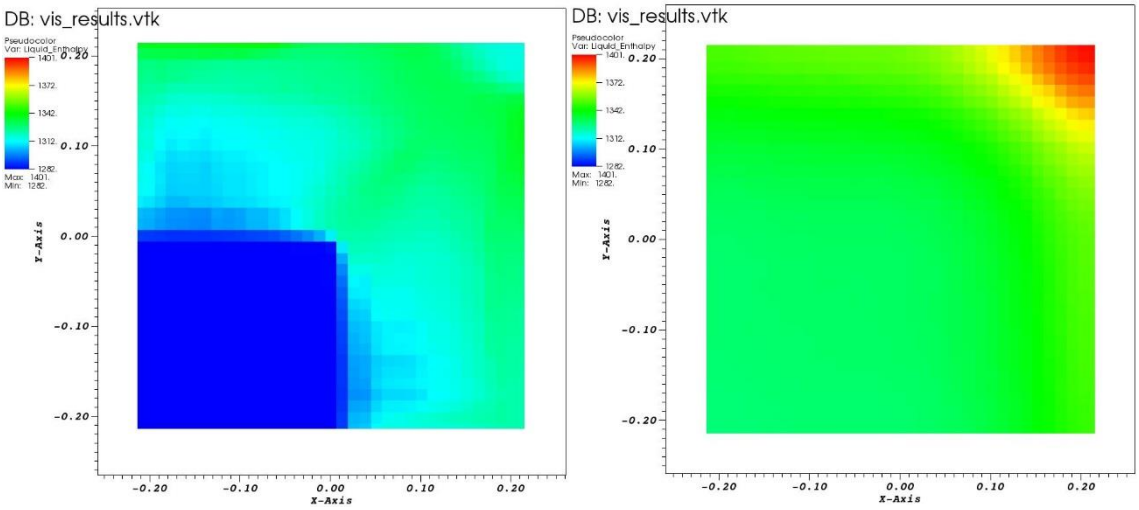

Figure 22. The inlet enthalpy plot (left) and outlet enthalpy plot (right) for the preliminary study.

The enthalpy distribution along the entire axial length of the model followed the predictions. The outside corner for assembly 3 is shown at the forefront of the left plot in Figure 23 and as predicted, stayed the coolest along the length of the entire core with respect to the rest of the model at the same axial height. The outside corner of assembly 2, shown at the forefront of the right plot in Figure 23, remained the hottest area of the

core along the length of the entire core with respect to the rest of the model at the same axial height.

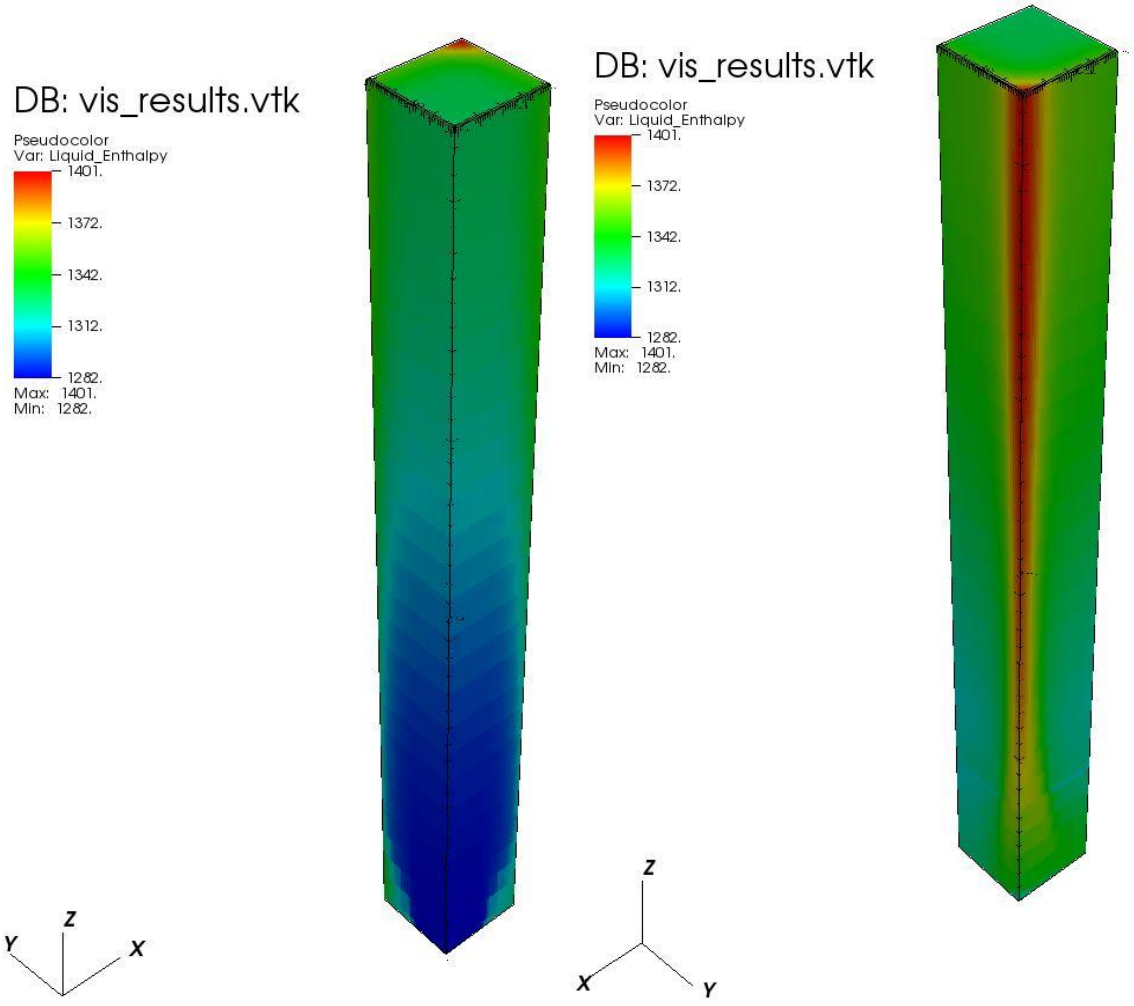

Figure 23. The enthalpy plot as viewed from the outside corner of assembly 3 (left) and the enthalpy plot as viewed from the outside corner of assembly 2(right) for the preliminary study.

The results from this preliminary study were encouraging and led to an optimistic outcome for large core simulations with blockage. However, it was later discovered that CTF may not be providing accurate results for running these simulations because in parallel mode, the input decks created for each assembly are such that the assembly geometries slightly overlap neighboring assemblies. Therefore, the channels at the periphery of each input deck for a parallel simulation will be shared among neighboring input decks. This means that changing the mass flow rate for the whole assembly creates a disagreement within the model by specifying two separate mass flow rates for some of the channels. This did not result in an error produced by CTF, however, as seen from the preliminary model. It does, however, provide skepticism for the results for blocked simulations. However, this should not hinder unblocked models where the mass flow rate or mass flux is not changing between assemblies. Therefore, the use of CTF for larger scale simulation that are not attempting to model blockage may still be reliable.

The average enthalpy across the model was verified by a hand calculation and showed great confidence. However, detailed results such as the hot channel are questionable due to this discovery. Furthermore, the cross flow and axial enthalpy/temperature profiles may be misleading as well. Another code was not able to be used at this time to help validate the CTF results to determine their accuracy, but this would be recommended in the future. This led to the creation of a serial simulation that attempted to model the same 2x2 problem. It was known that this would take a long time computationally, however, if successful, would address the concern.

The serial simulation was created successfully using the preprocessor and manually editing card 13 to address the inlet mass flow rates for each channel. When the simulation was run, it was never able to finish successfully; the reason for this is still unknown and being investigated. One possible reason is due to a convergence issue since the inlet mass flow rates have very abrupt changes within the serial model going from one cell to the next.

5.2 Troubleshooting and Limitations of CTF and Future Endeavors

The use of CTF revealed that this project was largely testing the usability of CTF for larger and more complex simulations. While CTF was successful at running steady-state models for single assemblies, it struggled with running larger simulations on multiple processors and more complex situations that required transient capabilities. CTF is designed for running transient simulations. Even steady-state simulations are pseudo-steady-state in that the simulation is actually run as a very short transient simulation that completes when convergence is reached. However, CTF lacks the ability to accurately model the RELAP5-3D simulation that was originally desired.

The mass flow rate would need to be changed over the course of the transient simulation, and at this time, this is not feasible with CTF. Furthermore, the preprocessor tool was not originally designed for aiding in the development of transient simulations. While this work has furthered the ability of the preprocessor tool to help facilitate the creation of transient simulations, there are still some features that need to be worked on further. Some of the limitations and bugs that were found have already been addressed during the course of this research (see Appendix C).

Another limitation for CTF is the way it runs in parallel mode. As discussed previously, CTF demands a large amount of computing resources to run in parallel mode. One processor is required for every assembly that is being modeled. This means to run a full core simulation for a 193 assembly PWR, 193 processors must be available for use. Furthermore, it seems that the perfection of parallel processing for CTF is still being worked on. As discussed earlier, in parallel mode, CTF creates the assembly input decks in a way that they slightly overlap each other. This creates an issue when trying to create blockage simulations in which the mass flow rate changes from assembly to assembly. This overlapping can create sub-channels that have disagreeing mass flow rates depending on the assembly input deck being viewed.

While significant advancements have been made to CTF, to increase its capability of performing both transient simulations and running in parallel, CTF is still not ready to be used for comparison with the RELAP5-3D simulation as originally intended. While a larger scale and more representative analysis was not completed, the preliminary findings as well as the advancements in the production of CTF holds hope for the future with this code. With the bugs that were found, it was determined that the analysis of blocked channels were unreliable on parallel processing and computational time and simulation crashes made them an invalid option for running in serial. Therefore, there is a lack of results for PWR simulations until more advancements have been made to CTF.

Research on this project will not cease though. While this phase of the project did not yield what was originally hoped for, it has laid the foundation for future work.

This project is already moving on by using a coarse lumping method with CTF in order to model an entire PWR core. This will be an attempt to try and model the RELAP5-3D simulation closer to the lumping scheme that was used originally. Once further advances have been made, a full core sub-channel model should still be looked at in order to verify that the lumping method used is appropriate and is not too coarse of a view of the reactor. One of the concerns is that too coarse of a lumping scheme might actually allow the code to inaccurately model in-core phenomena that occur such as backwards flow and circulation due to the blocked inlets. The findings from this work have cleared a path for this new approach and allow CTF to run more efficiently in transient and parallel simulations.

6. CONCLUSIONS

Significant advancements were made to CTF since the inception of this research. Parallel processing and even transient simulations were scarcely tested before these projects and significant contributions have been made to the advancement of these features from this research. In addition, the preprocessor tool has been improved and now allows for a much easier way to create transient simulations that allow the user to spend less time cross-checking the automation of the preprocessor. While there is still much to be done, CTF is well on its way to performing more difficult problems than steady-state simulations with uniform flow.

The advancements that were made from the commercial PWR analysis certainly aided in the success of the TRIGA analysis. The results from the TRIGA analysis in CTF have been compared with the STAR-CCM+ results and both show similar findings. It was discovered that natural convection correlations are not currently available in CTF but will be added in the future. Once this feature has been added, it would be a great opportunity for Texas A&M to revisit this work and validate the natural convection correlations with the CTF analytical model and STAR-CCM+ model that were found in this research. While STAR-CCM+ uses a film temperature along the wall of the fuel rods and CTF uses the bulk coolant temperature, the results from both codes do suggest that the coolant temperatures remain below 40°C sub-cooled.

Furthermore, it was shown that the insertion of the instrumentation tubes in the TRIGA core may aid in heat being extracted from the rods more efficiently. This

finding was counter-intuitive originally, but was explained upon further investigation. Both STAR-CCM+ and CTF results demonstrate that while there is less flow area for the coolant to fill within the sub-channels, the coolant is forced to flow in a closer proximity to the fuel rods allowing for less cross flow within each individual sub-channel. However, while the instrumentation tubes limit cross flow within each channel, it is apparent that they facilitate the movement of coolant from unblocked channels to blocked channels. Since the TRIGA core relies on natural convection, buoyancy is the driving force for the flow. It can be seen from both STAR-CCM+ and CTF results that the blocked channels have a significantly higher coolant temperature than the unblocked channels. Therefore, the less dense coolant within the blocked channels creates a driving force causing the coolant in surrounding channels with higher density to move towards the areas with lower density. Finally, it was seen in localized single pin tests that, in the blocked cases, the heat transfer coefficient is increased and this same phenomenon would be seen in the larger scale models as well. An increase in the heat transfer coefficient results in more efficient heat transfer between the fuel rod and the coolant.

These findings will be taken to the Reactor Safety Board and be presented in order to gain authorization to make the modifications in the core geometry. As CTF is improved, transient simulations of the TRIGA reactor can be made as well as eliminating the need for post processing data in order to obtain fuel rod temperature profiles. Once the modifications can be made to the reactor, empirical data can be collected to validate CTF rather than results from a CFD code.

CTF has not been thoroughly tested prior to use in these two projects. While it was initially thought to be a "ready to use" code, it was discovered that these projects tested the limitations of CTF. The feedback that has been received for the development of CTF from these two projects will greatly benefit the future users of CTF. With CTF's two-fluid, three-field model, its use in performing safety analyses for the nuclear industry will become very desirable as the code is improved.

REFERENCES

1. C. J. Shaffer, e.a., *GSI-191: Experimental Studies of Loss-of-Coolant-Accident-Generated Debris Accumulation and Head Loss with Emphasis on the Effects of Calcium Silicate Insulation*, U.S.N.R. Commission, Editor. 2005, U.S. Nuclear Regulatory Commission: Washington, DC.

2. T. S. Andreychek, e.a., *Evaluation of Long-Term Cooling Considering Particulate, Fibrous and Chemical Debris in the Recirculating Fluid*. 2011, Westinghouse: Cranberry Township, PA.

3. R. Vaghetto, Y.A.H., *Study of debris-generated core blockage scenarios during loss of coolant accidents using RELAP5-3D.* Nuclear Engineering and Design, 2013(261): p. 144-155.

4. D. L. Aumiller, E.T.T., R. C. Bauer, *Incorportation of COBRA-TF in an Integrated Code System with RELAP5-3D Using Semi-Implicit Coupling*, in *2002 RELAP5 Internantional Users Seminar*. 2002: Park City, Utah. p. 12.

5. Avramova, R.K.S.a.M.N., *CTF Theory Manual*. 2014A, The Pennsylvania State University.

6. C. M. Chance, J.V., J. C. Ragusa, *Steady-State Subchannel Analysis of Partially Blocked Coolant Channels in a Pool-Type TRIGA Reactor*, in *PHYSOR 2014*. 2014: Kyoto, Japan.

7. TEES, *Safety Analysis Report*, in *Texas Engineering Experiment Station*, T.A.M.U. System, Editor. 2011, Texas A&M University: College Station, TX.

8. Avramova, R.K.S.a.M.N., *CTF Pre-processor User's Manual*. 2014B, The Pennsylvania State University.

9. Wischnewski, B. *peace software*. http://www.peacesoftware.de/einigewerte/luft_e.html 2014 [cited 2014; Thermodynamic properties calculator for air (noncondensables)].

10. Kazimi, N.E.T.a.M.S., *Nuclear Systems I: Themal Hydraulic Fundamentals*. 1990: Hemisphere Publishing Corporation.

11. B. Tsuchiya, e.a., *Thermophysical properties of zirconium hydride and uranium-zirconium hydride.* Journal of Nuclear Materials, 2000. **289**.

12. Steel, A., *304/304L Stainless Steel Product Data Sheet*. 2007: West Chester, OH.

13. Doster, J.M., *Assessment of the Performance of COBRA-TF for the Prediction of Subcooled Boiling Conditions in Rod Bundles*, U.S.D.o. Energy, Editor. 2013.

14. Westinghouse, *Westinghouse AP1000 Design Control Document Rev. 19, Section 4.4*, U.S.N.R. Commission, Editor. 2011.

15. Westinghouse, *Westinghouse AP1000 Design Control Document Rev. 19, Section 4.1*, U.S.N.R. Commission, Editor. 2011.

16. Radulescu, J.C.W.a.G., *UO2 Fuel: Study of spent fuel compositions for long-term disposal*, in *Specification for Phase VII Benchmark*. 2009, ORNL: ORNL, USA.

Table A-1. Axial power profiles of all fuel rods in the TRIGA reactor.

ROD ID	POWER PER NODE (W)															ROD POWER
	NODE 1	NODE 2	NODE 3	NODE 4	NODE 5	NODE 6	NODE 7	NODE 8	NODE 9	NODE 10	NODE 11	NODE 12	NODE 13	NODE 14	NODE 15	(kW)
B3NW	390.9	328.1	376.0	398.0	421.5	428.3	434.2	416.8	413.0	387.1	361.5	323.9	285.8	246.9	276.4	5.4883
B3SW	457.0	422.0	465.8	506.8	538.9	522.2	533.0	522.5	503.9	474.7	433.1	382.0	335.9	288.7	302.3	6.6889
B3NE	409.2	363.5	400.2	430.0	446.9	450.5	449.9	436.0	428.6	399.4	384.9	354.3	302.6	286.6	292.2	5.8349
B3SE	459.4	414.5	453.6	480.0	513.3	526.1	505.9	495.8	464.8	431.4	412.0	369.4	315.3	265.4	285.0	6.3919
B4NE	628.7	575.8	629.8	666.2	678.8	662.3	635.1	620.7	576.8	545.0	487.4	450.1	381.1	329.3	317.8	8.1851
B4SE	662.1	608.5	689.2	711.6	708.7	658.8	607.2	569.0	549.3	491.5	444.1	414.8	343.3	280.0	292.9	8.0311
E5NW	992.0	951.7	1049.7	1139.7	1134.6	1045.8	982.5	928.5	884.1	806.7	734.2	641.0	566.7	476.5	454.4	12.7879
E5SW	995.8	922.6	1012.4	1102.1	1123.2	1142.5	1099.2	1056.1	984.2	911.2	831.7	729.0	643.1	521.2	507.7	13.5820
E5NE	965.6	904.9	991.1	1094.4	1108.8	1088.7	1051.5	990.1	947.5	897.9	804.6	719.6	627.9	517.2	502.7	13.2125
E5SE	957.3	881.9	1009.8	1118.0	1144.8	1128.4	1100.6	1061.4	1030.0	921.7	835.0	744.1	654.9	532.4	530.8	13.6512
B6NE	646.3	595.5	654.2	716.3	709.6	678.5	644.3	623.2	588.4	540.0	484.6	432.1	371.8	310.8	302.7	8.2982
B6SE	546.6	518.3	564.8	613.3	607.1	557.6	503.7	468.3	435.3	404.3	363.7	322.7	284.6	229.4	216.8	6.6366
F3NW	608.0	535.5	585.8	638.1	673.5	688.6	700.7	684.9	666.8	626.5	595.0	529.4	478.9	409.7	456.5	8.8777
F3SW	665.5	602.1	669.5	729.8	784.0	802.2	796.2	787.6	770.1	705.4	665.4	589.2	524.8	453.1	465.3	10.0102
F3NE	664.4	599.6	644.2	722.2	738.5	757.8	758.0	759.5	726.0	695.9	678.4	618.5	552.3	479.6	530.2	9.9250
F3SE	747.1	671.6	754.1	812.5	821.0	862.9	889.4	887.3	848.8	797.6	754.1	681.9	600.5	518.9	561.4	11.2091
B7NW	406.9	380.7	401.0	433.9	451.1	446.5	446.9	425.0	397.4	357.1	330.4	293.5	257.0	204.7	201.5	5.4334
B7SW	308.3	278.9	289.2	314.5	317.3	319.1	319.3	302.4	286.3	277.7	251.3	223.1	194.6	159.6	172.3	4.0139
B7NE	386.3	349.9	387.9	427.2	419.6	394.3	369.0	357.2	341.9	302.0	273.3	240.8	203.0	174.8	190.3	4.8176
B7SE	343.0	290.0	313.0	349.9	355.9	350.3	332.7	324.1	302.4	286.4	267.7	225.4	205.3	179.2	192.9	4.3181
B5NW	613.8	541.7	618.2	652.3	674.7	665.5	634.8	643.9	603.5	548.6	482.7	448.5	375.6	317.1	321.4	8.1423
B5SW	596.4	526.9	581.5	620.2	638.5	645.1	628.7	614.5	569.6	534.6	480.9	422.9	371.4	305.5	322.0	7.8586
B5NE	608.0	550.1	619.5	630.0	666.7	626.2	604.1	573.9	552.7	518.2	443.4	402.2	349.2	293.1	303.7	7.7411
B5SE	594.5	551.3	591.7	624.1	640.5	629.2	618.5	602.0	545.1	510.7	464.9	408.5	344.6	302.1	308.6	7.7362
C3NW	498.7	456.7	489.8	533.6	533.6	557.9	573.5	549.4	530.5	501.2	473.1	428.4	383.1	326.6	351.7	7.1880
C3SW	547.9	501.7	572.5	610.7	613.7	637.7	614.4	583.7	576.3	522.7	481.6	439.4	388.2	326.2	332.9	7.7497
C3NE	716.6	654.2	730.1	776.8	806.6	853.5	829.1	823.9	784.2	751.0	703.6	641.6	558.4	476.5	503.2	10.6092
C3SE	796.4	743.7	837.6	924.0	939.3	946.8	934.5	901.7	861.5	800.2	742.6	673.6	583.5	499.4	498.6	11.6835
E3NW	793.1	745.6	812.0	885.8	932.7	944.2	945.6	930.0	911.3	847.7	779.9	706.8	614.3	554.4	575.2	11.9787
E3SW	898.9	863.7	961.5	1027.6	1065.9	1073.5	1086.6	1034.1	1001.4	936.3	858.3	756.8	659.2	570.7	572.5	13.3670
E3NE	629.4	566.6	626.7	681.9	702.1	720.6	725.1	709.6	679.2	643.8	602.2	547.5	513.3	434.5	477.9	9.2602
E3SE	716.4	647.6	724.8	794.7	826.0	828.7	846.5	822.6	787.2	733.2	667.7	627.9	516.3	453.1	478.5	10.4712
C7NW	486.9	443.4	487.5	506.0	500.8	462.9	403.9	386.3	371.4	327.0	309.9	257.6	229.7	187.5	194.4	5.5555

Table A-1. Continued

ROD ID	POWER PER NODE (W)															ROD
	NODE 1	NODE 2	NODE 3	NODE 4	NODE 5	NODE 6	NODE 7	NODE 8	NODE 9	NODE 10	NODE 11	NODE 12	NODE 13	NODE 14	NODE 15	POWER
C7SW	413.0	361.6	406.6	435.7	442.0	434.0	414.7	402.3	379.5	351.7	317.7	289.2	244.0	202.3	217.8	5.3120
C7NE	700.6	666.5	739.6	767.8	774.3	760.3	719.2	678.6	634.8	607.7	538.9	496.2	410.4	334.2	338.8	9.1679
C7SE	608.9	570.5	642.2	690.7	700.1	694.9	688.3	652.6	594.0	572.8	516.8	447.5	393.1	322.1	332.7	8.4271
F4NW	792.4	697.7	799.8	914.6	927.8	945.0	938.9	913.5	868.8	822.8	764.9	686.6	614.3	506.6	529.6	11.7231
F4SW	865.7	790.8	884.1	967.7	1017.6	1026.6	1001.2	974.4	925.6	856.5	799.1	725.7	625.7	524.4	539.1	12.5241
F4NE	853.0	758.9	864.5	947.9	997.5	1011.3	1020.2	1023.1	987.6	929.7	861.3	777.8	688.9	598.8	633.8	12.9542
F4SE	931.0	831.1	945.5	1031.5	1091.1	1103.6	1115.4	1077.9	1043.2	987.7	917.3	831.3	759.8	625.7	669.5	13.9619
D4NW	975.3	886.6	970.7	1063.1	1105.3	1091.3	1086.7	1039.5	977.8	911.8	836.8	744.2	657.1	554.2	540.5	13.4410
D4SW	898.9	841.9	927.8	992.9	1014.8	1013.0	987.3	934.3	863.8	820.5	748.7	660.7	560.0	461.5	448.7	12.1747
D4NE	991.2	932.2	1055.1	1116.6	1137.0	1124.3	1063.8	1019.5	985.5	908.8	831.1	766.0	652.0	539.7	530.0	13.6528
D4SE	940.5	902.6	995.0	1087.7	1054.3	958.0	877.8	842.1	784.6	736.6	693.5	591.5	521.7	437.0	399.7	11.8224
E7NW	866.1	802.7	914.8	928.0	904.8	858.3	791.3	757.9	678.7	617.3	549.4	497.9	420.1	355.9	329.5	10.2727
E7SW	735.0	683.8	764.8	788.9	824.9	826.5	816.4	765.4	725.0	649.6	572.7	516.9	457.3	392.8	381.1	9.9011
E7NE	834.1	768.6	830.3	904.5	945.4	917.2	896.2	806.0	715.5	557.8	439.5	371.3	312.8	265.2	264.1	9.8284
E7SE	620.4	562.4	613.1	638.1	660.7	668.1	646.2	603.4	570.8	500.9	437.4	389.1	331.3	277.5	295.0	7.8146
F8NW	487.4	440.6	480.6	496.2	528.2	531.4	537.7	519.8	475.0	438.8	411.0	349.3	316.9	271.6	295.4	6.5798
F8SW	422.1	382.4	409.7	421.6	453.1	461.8	445.5	439.9	418.5	402.4	373.1	324.5	288.2	263.9	284.0	5.7906
F8NE	524.5	461.7	508.5	532.6	555.5	573.4	580.3	559.9	542.3	495.1	462.0	397.0	371.1	310.6	339.6	7.2141
F8SE	452.4	386.4	420.5	447.0	471.4	468.9	468.1	456.8	439.7	421.3	397.3	347.9	312.0	288.7	309.6	6.0878
F5NW	888.7	822.2	950.5	1039.7	1051.6	1090.3	1057.0	1037.8	975.2	927.0	823.9	731.9	657.8	530.8	554.0	13.1385
F5SW	911.3	842.8	962.9	1010.5	1038.1	1060.5	1062.5	1028.8	960.9	896.4	799.6	728.4	635.7	541.4	552.8	13.0326
F5NE	956.2	870.9	983.5	1067.7	1122.3	1145.8	1149.1	1136.0	1074.2	1021.4	939.8	857.9	740.4	645.5	671.2	14.3819
F5SE	963.2	861.0	979.4	1041.0	1118.0	1115.5	1120.9	1101.5	1038.9	996.9	911.4	808.2	725.5	622.0	655.9	14.0591
F6NW	860.6	779.1	856.7	925.0	957.6	984.7	954.5	928.4	891.2	804.4	740.1	647.9	562.4	468.8	486.3	11.8477
F6SW	853.7	765.3	856.0	934.1	972.6	973.5	945.1	887.1	806.3	669.9	564.5	487.7	407.9	330.7	350.4	10.8046
F6NE	909.2	840.5	917.9	978.9	1044.1	1045.2	1030.7	1008.4	966.2	903.7	844.7	717.5	660.0	553.6	591.1	13.0117
F6SE	838.9	747.4	840.2	912.0	941.8	959.0	951.8	909.6	848.6	783.0	677.9	610.7	532.7	452.1	493.4	11.4991
C5NW	739.7	676.2	752.7	807.2	802.5	757.8	708.1	659.2	615.2	578.7	525.2	454.9	392.7	326.2	313.9	9.1102
C5SW	727.9	678.4	752.5	831.1	838.8	834.2	816.5	772.3	723.9	688.6	615.6	544.1	457.1	374.3	374.5	10.0297
C5NE	896.1	832.3	946.7	984.3	997.6	976.7	941.5	922.4	876.2	812.2	707.5	633.7	541.4	463.1	412.9	11.9447
C5SE	988.6	909.4	996.0	1055.7	1098.7	1103.5	1072.6	1016.1	963.5	921.0	826.2	725.6	606.7	510.2	440.6	13.2344
D6NW	952.3	867.2	946.1	1024.3	1048.7	1043.2	1030.5	983.0	915.6	836.9	768.6	679.4	580.2	483.8	430.4	12.5902
D6SW	885.6	805.4	907.9	962.9	974.4	980.8	931.0	895.6	836.4	780.9	713.3	611.0	527.2	440.8	426.9	11.6798

Table A-1. Continued

ROD ID	POWER PER NODE (W)															ROD POWER
	NODE 1	NODE 2	NODE 3	NODE 4	NODE 5	NODE 6	NODE 7	NODE 8	NODE 9	NODE 10	NODE 11	NODE 12	NODE 13	NODE 14	NODE 15	
D6NE	908.8	819.7	951.4	993.5	1013.2	1003.6	959.0	913.8	849.1	798.0	699.7	640.3	555.2	455.2	413.6	11.9740
D6SE	893.3	844.3	961.0	1012.8	999.7	935.2	841.8	789.2	721.6	687.5	627.6	553.0	459.9	381.3	352.9	11.0611
D5NW	1076.4	1013.7	1099.8	1146.6	1206.9	1203.0	1190.0	1125.9	1076.0	988.2	877.5	781.0	674.8	556.0	476.2	14.4921
D5NE	1032.7	981.0	1076.4	1135.0	1197.6	1145.0	1113.0	1065.7	1010.6	893.0	823.1	731.6	635.5	534.0	496.6	13.8707
D5SE	1130.9	1021.0	1145.3	1228.4	1253.0	1259.3	1219.6	1188.8	1114.5	1011.6	908.4	808.0	701.3	576.4	519.6	15.0863
D5SW	0.0	0.0	0.0	0.0	0.0	0.0	0.0	0.0	0.0	0.0	0.0	0.0	0.0	0.0	0.0	0.0000
E6NW	912.9	863.7	970.3	1017.4	1041.0	988.6	902.8	845.1	787.8	732.9	661.8	607.4	501.1	407.1	395.5	11.6355
E6SW	46.8	39.6	47.3	76.3	137.7	235.3	358.6	450.3	534.2	540.5	534.5	582.9	653.2	654.5	533.0	5.4249
E6NE	920.8	830.6	967.0	1022.5	1037.8	1031.4	986.7	947.9	886.8	828.3	720.0	643.4	566.5	453.6	447.9	12.2913
E6SE	792.0	775.7	849.0	911.8	903.3	851.7	773.4	729.0	668.0	592.3	516.6	451.6	373.8	310.5	311.6	9.8101
C6NW	657.7	611.6	680.7	736.7	736.5	681.7	643.5	608.1	566.2	533.9	471.9	419.2	351.6	301.5	289.4	8.2904
C6SW	32.3	34.7	37.7	56.7	98.0	172.1	256.4	334.5	388.6	375.4	358.8	407.5	439.8	451.7	372.5	3.8168
C6NE	795.5	721.5	799.5	863.9	885.7	878.2	831.3	779.4	754.3	684.2	629.6	562.1	463.7	395.6	362.6	10.4071
C6SE	672.0	618.8	690.0	705.7	722.4	664.9	639.3	589.6	559.0	521.2	462.4	418.2	346.3	281.3	277.8	8.1689
C4NW	580.1	586.5	633.5	654.0	656.0	611.7	574.7	534.0	513.4	476.1	441.0	379.3	342.6	264.8	274.2	7.5218
C4SW	35.0	34.3	36.5	66.9	117.6	201.7	301.8	386.5	452.3	444.9	454.7	502.5	550.8	566.9	444.6	4.5970
C4NE	737.9	682.6	737.2	816.2	820.1	814.8	776.2	734.0	721.2	651.9	615.2	540.8	460.2	388.1	396.0	9.8924
C4SE	778.5	739.5	829.7	866.9	862.2	823.7	761.4	721.4	671.0	626.9	570.4	517.9	446.5	387.5	346.6	9.9502
E4NW	789.7	758.5	844.1	889.3	904.8	830.7	794.2	738.8	689.6	626.6	586.9	527.3	466.7	388.8	375.8	10.2119
E4SW	45.8	44.8	50.8	89.9	153.1	267.7	404.2	507.3	596.1	608.9	621.7	688.6	758.3	779.9	623.1	6.2402
E4NE	795.5	760.9	833.4	894.3	920.3	926.2	890.2	859.8	798.5	746.2	668.5	632.6	558.0	453.0	461.8	11.1991
E4SE	888.3	841.6	946.3	1002.8	1001.2	933.9	849.9	819.6	775.4	741.5	665.2	600.4	521.3	414.8	425.2	11.4275
F7NW	640.0	575.5	652.6	716.2	756.4	748.5	718.1	686.8	632.3	482.1	383.7	329.3	285.1	241.1	250.2	8.0979
F7NE	866.7	788.7	876.7	962.7	983.5	1022.6	1007.5	968.6	877.3	711.1	599.0	521.0	464.9	382.1	401.9	11.4343
F7SE	664.7	583.9	635.4	679.8	720.0	739.5	721.2	696.6	658.7	576.2	508.9	452.3	387.1	344.5	363.1	8.7318
F7SW	0.0	0.0	0.0	0.0	0.0	0.0	0.0	0.0	0.0	0.0	0.0	0.0	0.0	0.0	0.0	0.0000

Figure A-1 and Figure A-2 are the unblocked and blocked radial temperature profiles of rod C5SE in the TRIGA reactor, respectively. Figure A-3 and Figure A-4 are the unblocked and blocked radial temperature profiles of rod D4SW in the TRIGA reactor, respectively. Each figure shows both the CTF analytical model as well as the STAR-CCM+ model.

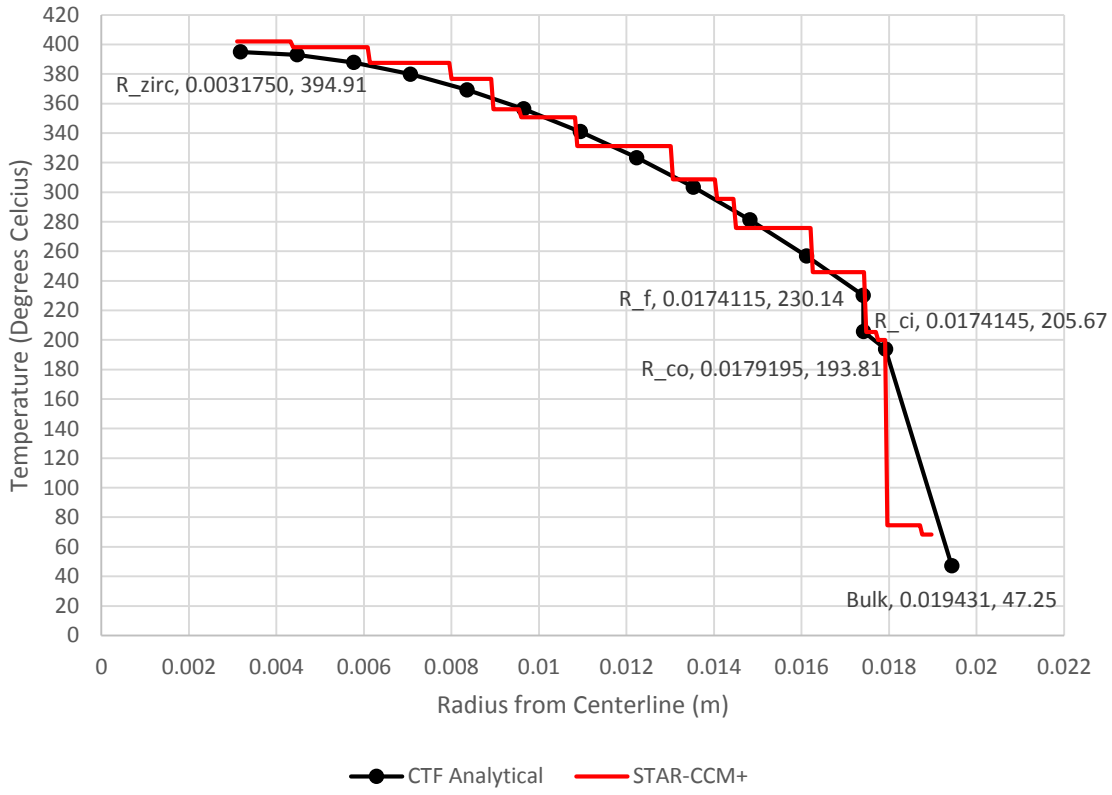

Figure A-1. The comparison of STAR-CCM+ and CTF analytical unblocked radial temperature profiles for fuel rod C5SE at an axial height of 0.191m (just above core centerline).

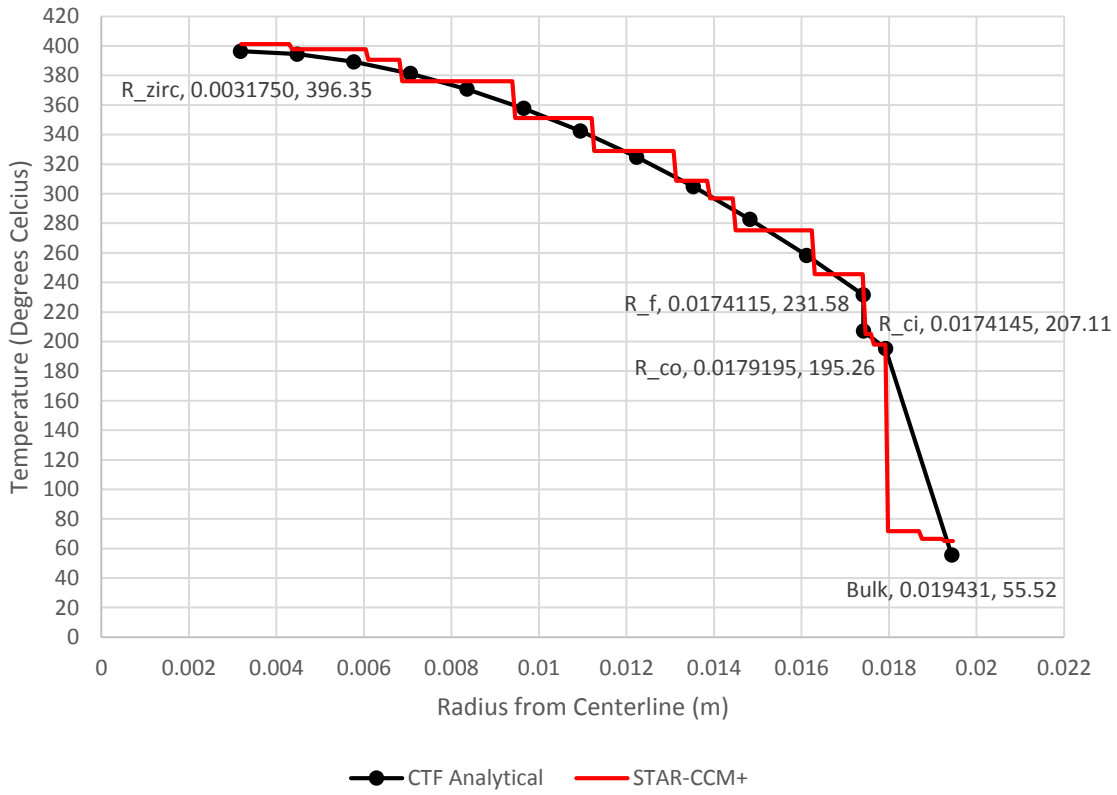

Figure A-2. The comparison of STAR-CCM+ and CTF analytical blocked radial temperature profiles for fuel rod C5SE at an axial height of 0.191m (just above core centerline).

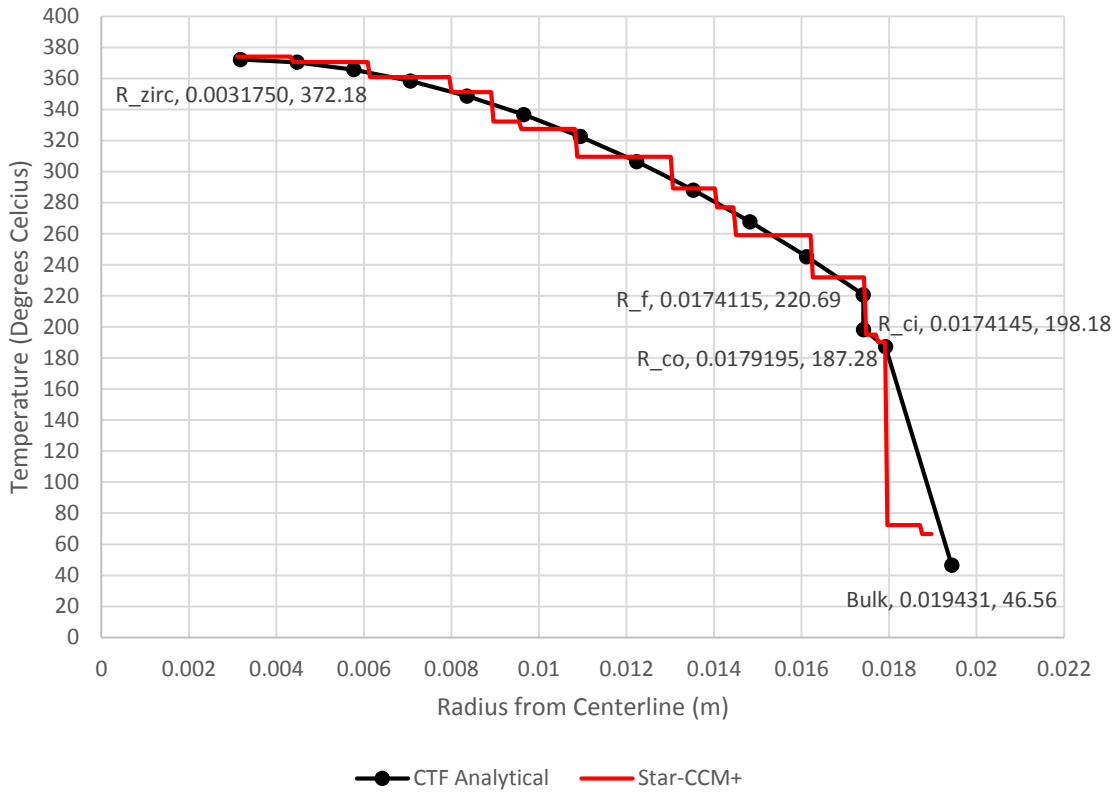

Figure A-3. The comparison of STAR-CCM+ and CTF analytical unblocked radial temperature profiles for fuel rod D4SW at an axial height of 0.191m (just above core centerline).

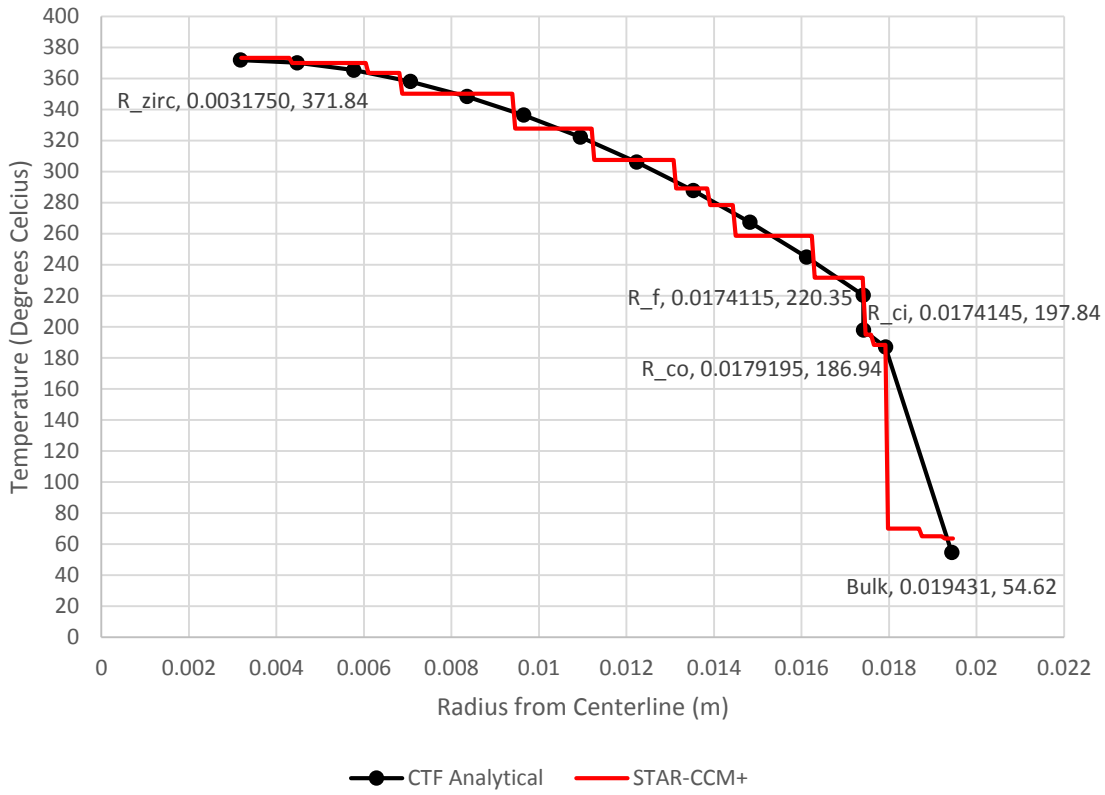

Figure A-4. The comparison of STAR-CCM+ and CTF analytical blocked radial temperature profiles for fuel rod D4SW at an axial height of 0.191m (just above core centerline).

APPENDIX B

This appendix contains examples of the input decks for both CTF and the preprocessor tool. The input decks shown here are the input decks used for the single pin, unblocked model of rod D4SW in the TRIGA reactor. The first input deck is the control.inp deck used for the preprocessor, the second input deck is the geo.inp deck used for the preprocessor, the third input deck is the assembly.inp deck (renamed pin.inp for this particular simulation) for the preprocessor, the fourth input deck is the power.inp deck for the preprocessor, and the fifth and final input deck is deck.inp for CTF (after manual modifications that were necessary). Each input deck will be separated by a page break and a bold line in 12pt font that will title the input deck that follows.

CONTROL.INP

```
*****************************************************
*                  Main control data                *
*****************************************************
*Title for deck (max 30 characters)
TRIGA_Pin11471_Unblocked
*Setup problem for parallel solution?
{parallel}
*no - not parallel
*yes - parallel
no
*Print Rod/Channel map data to Group 17 on deck.inp?
** MAPS = 1 -- yes
** MAPS = 0 -- no
** MAPS
1
** Name for the HDF5 file - enter if MAPS=1
TRIGA_Pin11471_Unblocked
** Name for the VTK file - enter if MAPS=1
TRIGA_Pin11471_Unblocked
**
*Number of transient power files
*Defaults to 1 if omitted from this deck
*{num transient power files}
*1
*Units options
**0 - US input / SI output*
**1 - SI input / SI output*
**2 - US input / US output*
**3 - SI input / US output*
1
* EPSO
0.001
* OITMAX
5
* IITMAX
40
**Courant
0.8
**************************
*        MODELS          *
```

```
*************************
*
****************************************
*     Rod friction factor correlation     *
****************************************
**1 -- original correlation
**2 -- COBRA-3C
**3 -- FLICA-4
2
****************************************
*    Entrainment and deposition model     *
****************************************
**0 -- neither entrainment nor deposition
**1 -- original model
****************************************
0
*************************************************************************
*                   Mixing and void drift model                         *
*************************************************************************
**0 -- neither mixing nor void drift
**1 -- user specified constant (two-phase)turbulent mixing coeff.
**2 -- single-phase mixing coeff. according to Rogers and Rosehart
**3 -- user specified constant single-phase turbulent mixing coeff.
*************************************************************************
*IMIX
0
*************************************************************************
*        MIXING/VOID DRIFT PARAMETERS - skip if IMIX=0             *
*************************************************************************
**AAAK - Equilibrium distribution weighting factor Km in
**void drift model (0.0 void drift inactive / 1.4 suggested value)
**Enter for IMIX=1, 2, and 3
*0.0
**BETA  - Constant mixing coefficient, Enter for IMIX=1 and 3
**Mixing coefficient for two-phase if IMIX=1
**Mixing coefficient for single-phase if IMIX=3
*0.00
**DFROD - Outside rod diameter, Enter only for IMIX=2
*9.5e-3
**THETM - Ratio between maximun two-phase turbulent mixing coeff.
**and single-phase turbulent mixing coeff.
**Enter only for IMIX=2 and 3
**5.0
*
**************************************
*             Solver                 *
**************************************
**0 -- Direct Gaussian
**1 -- BSGS with ILUT preconditioner
**2 -- GMRES with no preconditioner
**3 -- BSGS with no preconditioner
**4 -- GMRES with ILUT preconditioner
**************************************
0
*
****************************************
*         INITIAL CONDITIONS           *
****************************************
*Initialization mass flow rate (kg/s)
0.0785
*Initialization temperature for the rods (C)
206.8
*Reference pressure (bar)
1.8
*Reference enthalpy (kJ/kg)
-30.0
*Reference enthalpy for noncondesables (kJ/kg)
*http://www.peacesoftware.de/einigewerte/luft_e.html
303.464
*Fraction of heat produced by rods that is
*released directly to the coolant
```

```
0.0
****************************************
*      GLOBAL BOUNDARY CONDITIONS       *
****************************************
**
************************************
*      BOUNDARY CONDITION TYPE      *
************************************
**1 -- pressure and enthalpy
**2 -- mass flow rate and enthalpy
**3 -- mass flow rate only
**4 -- mass source
**5 -- pressure sink
************************************
*Inlet boundary condition type
2
*Outlet boundaty condition type
1
************************************
*      BOUNDARY CONDITION VALUES      *
************************************
*Total inlet mass flow rate (kg/s)
*Only if BC type is 2 or 3 at inlet (0.0 otherwise)
0.0785
*Inlet Enthalpy (kJ/kg}
*Only if BC type is 1 or 2 at inlet (0.0 otherwise)
-30.0
*Outlet Enthalpy (kJ/kg}
*Only if BC type is 1 or 2 at outlet (0.0 otherwise)
271.3
*Inlet Pressure (bar)
*Only if BC type is 1 or 5 at inlet (0.0 otherwise)
0.0
*Outlet Pressure (bar)
*Only if BC type is 1 or 5 at outlet (0.0 otherwise)
1.8
************************************
*      Time Domain Data              *
************************************
{run as transient}
*yes - run as transient
*no - run as steady-state
no
*DTMIN
0.00001
*DTMAX
1.0
*TEND
0.0
*RTWFP
1000.0
*MAXITS
10000
************************************
*      Convergence Data              *
************************************
{convergence criteria}
*Global Energy Balance (%) - default is 0.01
0.01
*Global Mass Balance (%) - default is 0.01
0.01
*Fluid Energy Storage (%) - default is 0.5
0.5
*Solid Energy Balance (%) - default is 0.5
0.5
*Mass Storage (%) - default is 0.5
0.5
************************************
*     Output Options                 *
************************************
*0 - Do not print data
```

```
*1 - Print data
{edit channels}
1
{edit gaps}
1
{edit rods}
1
{edit dnb}
1
{rods vtk}
1
```

GEO.INP

```
*0 represnets void
*number of fuel assemblies
1
*NUMBER OF FUEL ASSEMBLY TYPES:
1
*DIMENSION OF CORE MESH (columns (x),rows (y)):
1 1
{model shroud}
no
*OPTION FOR CORE MODELING
** 1 = Model as shown in the following map
** 4 = Model using quarter core symmetry
** 8 = Model using eighth core symmetry
** Note: If using options 4 or 8, make a map of
**       the full core and the preprocessor will
**       take care of breaking it down into quarter
**       or eighth symmetry
{symmetry option}
1
*FUEL ASSEMBLY MAP
***1  2
1  1
*AXIAL MESH INFORMATION
*Number of axial groups
14
*Z(mm) top of group   Number of Scalar Cells from last zone to this point
     27.21428571      1
     54.42857143      1
     81.64285714      1
     108.8571429      1
     136.0714286      1
     163.2857143      1
     190.5000000      1
     217.7142857      1
     244.9285714      1
     272.1428571      1
     299.3571429      1
     326.5714286      1
     353.7857143      1
     381.0000000      1
*Note that you must put the top of the model as the last group
*ALLOCATION OF FUEL TYPES
pin.inp
```

PIN.INP (COMMONLY REFERED TO AS ASSEMBLY.INP)

```
*********************************************
*          FUEL ASSEMBLY PARAMETERS         *
*********************************************
*
**************************************
*  General parameter of fuel assembly  *
**************************************
*
*Numer of fuel rods
1
*Size of fuel array
1
*Number of guide tubes/water rods
0
*Active length (mm)
381
{active region start}
0.0
*Bundle pitch (mm)
38.862
*Walls around bundle?
**0=No
**1=Yes
0
**
*Type of heated elements
**0=Nuclear Fuel Rods
**1=Electric Heater Tubes
0
************************************************
*        Cladding and fuel pellet parameters      *
**DO NOT ENTER IF THERE ARE NO NUCLEAR FUEL RODS  *
************************************************
*
*Conduction Model Flag
1
*Fuel pellet diameter (mm)
34.823
*Radial nodes in the fuel pellet
10
*Cladding inner diameter (mm)
34.829
*Cladding outer diameter (mm)
35.839
*Pin pitch (mm)
38.862
*Therical density of the fuel pellet (%) (/ i.e.: 95%)
95.0
*Constant gap conductance of the gas (W/m**2-K)
15764
*Cladding material
SS304
*
************************************************
*            Heater Tube Parameters            *
**DO NOT ENTER IF NO ELECTRIC HEATER RODS         *
************************************************
***
***Tube inside diameter (mm)
**8.2
***Tube outside diameter (mm)
**9.5
***Tube pitch (mm)
**12.6
****
****************************************
*   Guide tubes / water rods parameters  *
**DO NOT ENTER IF NO GUIDE TUBES         *
```

```
****************************************
*
*Inner diameter of guide tube/water rod (mm)
*11.22
*Outer diameter of guide tube/water rod  (mm)
*12.04
*Guide tube/water rod material
*Zircaloy
*Guide tube positions in the fuel lattice starting from lower left corner
*Use X Y format
*****************************
*      Spacer grids data     *
*****************************
*
*Number of spacer grids
0
*Sp.grid  Initial height (mm)    Minor loss coefficient /Heights refered to the beginning of
active fuel (BAF)/
```

POWER.INP

```
************************************************
*       TOTAL POWER AND POWER PROFILES         *
************************************************
*
******************
*   Total power  *
******************
*
* Flag / core (0) o fuel (1)/
*0
*Time at which this power profile is applied (seconds)
*{transient time}
*0
* Power in MWth for total number of fuel assemblies
0.012846
*
************************
*    Power profiles    *
************************
*
* Number of pairs (height/relative power) of axial profile /Heights refered to the beginning of
active fuel (BAF)/
15
*  Height (mm)      Relative power
    0.000000000      0.552788311
    27.21428571      0.568613775
    54.42857143      0.689965978
    81.64285714      0.813965675
    108.8571429      0.922480854
    136.0714286      1.010916733
    163.2857143      1.064310512
    190.5000000      1.151071399
    217.7142857      1.216412077
    244.9285714      1.248053852
    272.1428571      1.250273445
    299.3571429      1.223265354
    326.5714286      1.143151803
    353.7857143      1.037279540
    381.0000000      1.107450691
*******************************
*Core Radial Power Factors
*******************************
**This specifies the power factors to be
**applied to each whole assembly.  Values
**must normalize to one.
1.0
*******************************
*Assembly Radial Power Factors*
*******************************
**This specifies the power factors to be
**applied within each assembly (i.e., to
**each rod in the assembly).  Make sure
**there is one value per rod.  Guide tubes
**should get a value of zero.  Also, this
**must normalize to one.
**      1
1.0000000
```

DECK.INP

```
*****************************************************************************************************
*MAIN CONTROL DATA
*****************************************************************************************************
*ICOBRA
      1
*INITIAL   DUMPF
       1       0
**    EPSO    OITMAX    IITMAX   COURANT
  0.001000         5        40  0.800000
*TITLE
TRIGA_Pin11471_Unblocked
*****************************************************************************************************
*GROUP 1 - Calculation Variables and Initial Conditions                                             *
*****************************************************************************************************
**NGR
   1
**NGAS IRFC EDMD IMIX ISOL          GINIT NOTRN MESH MAPS IPRP MFLX NM12 NM13 NM14
     1    2    0    0    0  0.7850000E-01     1    1    1    0    0    0    0    0
*Card 1.2
**         GTOT           AFLUX          DHFRAC           MFLUX
  0.7850000E-01  0.3371654E+02  0.0000000E+00
*Card 1.3
**         PREF            HIN            HGIN          VFRAC1          VFRAC2
      1.8000000    -30.0000000    303.4640000       1.0000000       0.9999000
*Card 1.4
**GTP(1)   VFRAC(3)  GTP(2) VFRAC(4)  GTP(3) VFRAC(5)  GTP(4) VFRAC(6)
     air     0.0001
*****************************************************************************************************
*GROUP 2 - Channel Description                                                                      *
*****************************************************************************************************
**NGR
    2
*Card 2.1
**  NCH NDM2 NDM3 NDM4 NDM5 NDM6 NDM7 NDM8 NDM9 NM10 NM11 NM12 NM13 NM14
      4    0    0    0    0    0    0    0    0    0    0    0    0    0
*Card 2.2
**   I           AN           PW ABOT ATOP NMGP           X           Y        XSIZ        YSIZ
     1 0.12537E-03 0.28148E-01    0    0    0 -0.97155E-02  0.97155E-02  0.19431E-01  0.19431E-
01
     2 0.12537E-03 0.28148E-01    0    0    0  0.97155E-02  0.97155E-02  0.19431E-01  0.19431E-
01
     3 0.12537E-03 0.28148E-01    0    0    0 -0.97155E-02 -0.97155E-02  0.19431E-01  0.19431E-
01
     4 0.12537E-03 0.28148E-01    0    0    0  0.97155E-02 -0.97155E-02  0.19431E-01  0.19431E-
01
*****************************************************************************************************
*GROUP 3 - Transverse Channel Connection (Gap) Data
*****************************************************************************************************
**NGR
    3
*Card 3.1
**  NK NDM2 NDM3 NDM4 NDM5 NDM6 NDM7 NDM8 NDM9 NM10 NM11 NM12 NM13 NM14
     4    0    0    0    0    0    0    0    0    0    0    0    0    0
*Card 3.2
**   K    IK    JK        GAP        LNGT  WKR FWAL IGPB IGPA FACT IGAP JGAP IGAP JGAP IGAP JGAP
*Card 3.3
**GMULT   ETNR
     1     1     2  0.151E-02  0.194E-01  0.5  0.0    0    0  1.0    0    0    0    0    0    0
      1    0.0
     2     1     3  0.151E-02  0.194E-01  0.5  0.0    0    0  1.0    0    0    0    0    0    0
      1    0.0
     3     2     4  0.151E-02  0.194E-01  0.5  0.0    0    0  1.0    0    0    0    0    0    0
      1    0.0
     4     3     4  0.151E-02  0.194E-01  0.5  0.0    0    0  1.0    0    0    0    0    0    0
      1    0.0
*Card 3.3.5
**   K            X            Y      NORM
     1  0.00000E+00  0.97155E-02     x
```

```
     2 -0.97155E-02  0.00000E+00     y
     3  0.97155E-02  0.00000E+00     y
     4  0.00000E+00 -0.97155E-02     x
*Card 3.4
**NLGP
     0
*****************************************************************************************
*GROUP 4 - Vertical Channel Connection Data                                             *
*****************************************************************************************
**NGR
    4
*Card 4.1
**NSEC NSIM IREB NDM4 NDM5 NDM6 NDM7 NDM8 NDM9 NM10 NM11 NM12 NM13 NM14
     1    1    0    0    0    0    0    0    0    0    0    0    0    0
*Card 4.2
**ISEC    NCHN  NONO         DXS     IVAR
     1       4    14 0.27214E-01       14
*Card 4.3
**JLEV       VARDX  JLEV       VARDX  JLEV       VARDX  JLEV       VARDX  JLEV       VARDX
     2 0.27214E-01     3 0.27214E-01     4 0.27214E-01     5 0.27214E-01     6 0.27214E-01
     7 0.27214E-01     8 0.27214E-01     9 0.27214E-01    10 0.27214E-01    11 0.27214E-01
    12 0.27214E-01    13 0.27214E-01    14 0.27214E-01    15 0.27214E-01
*Card 4.4
**    I   KCHA  KCHA  KCHA  KCHA  KCHA  KCHA   KCHB  KCHB  KCHB  KCHB  KCHB  KCHB
      1      1     0     0     0     0     0      1     0     0     0     0     0
      2      2     0     0     0     0     0      2     0     0     0     0     0
      3      3     0     0     0     0     0      3     0     0     0     0     0
      4      4     0     0     0     0     0      4     0     0     0     0     0
*Card4.5
**  IWDE
      4
*Card 4.6
**  MSIM
     56
*****************************************************************************************
*GROUP 7 - Grid Loss Coefficient Data                                                   *
*****************************************************************************************
**NGR
    7
*Card 7.1
**  NCD NGT  IFGQF IFSDRP  IFESPV  IFTPE  IGTEMP  NFBS  NDM9 NDM10 NDM11 NDM12 NDM13 NDM14
      0   0      0      0       0      0       0     0     0     0     0     0     0     0
*Card 7.2
**   CDL    J   CD1   CD2   CD3   CD4   CD5   CD6   CD7   CD8   CD9  CD10  CD11  CD12
*****************************************************************************************
*GROUP 8 - Rod and Unheated Conductor Data                                              *
*****************************************************************************************
**NGR
    8
*Card 8.1
** NRRD   NSRD    NC  NRTB  NRAD  NLTY  NSTA   NXF  NCAN  RADF    W3 NDM12 NDM13 NDM14
     1      0     1     1     0     0     1     1     0     0     0     0     0     0
*Card 8.2
**    N   IFTY   IAXP   NRND DAXMIN  RMULT        HGAP  ISECR  HTAMB   TAMB
*Card 8.3
**NSCH   PIE  NSCH   PIE  NSCH   PIE  NSCH   PIE  NSCH   PIE  NSCH   PIE  NSCH   PIE NSCH   PIE
     1      1     1      0      0  1.000 0.15764E+05      1  0.000  0.000
     3 0.250     4 0.250     1 0.250     2 0.250     0 0.000     0 0.000     0 0.000     0
0.000
*Card 8.6
**    I   NRT1   NST1   NRX1
      1      1      0      2
*Card 8.7
**IRTB1  IRTB2  IRTB3  IRTB4  IRTB5  IRTB6  IRTB7  IRTB8  IRTB9 IRTB10 IRTB11 IRTB12
      1
*Card 8.9
**    AXIALT      TRINIT
 0.00000E+00 0.20680E+03
 0.38100E+00 0.20680E+03
*****************************************************************************************
*GROUP 9 - Conductor Geometry Description                                               *
```

```
*****************************************************************************************
**NGR
    9
*Card 9.1
** NFLT IRLF ICNF IMWR NDM5 NDM6 NDM7 NDM8 NDM9 NM10 NM11 NM12 NM13 NM14
      1    0    0    0    0    0    0    0    0    0    0    0    0    0
*Card 9.2
**  I FTYP        DROD        DFUL  NFUL IMTF IMTC IMOX DCRE       TCLD  FTDS IGPC IGFC IRDP
    1 nucl 0.03583900 0.03482300    10    1    2    0 0.00 0.505E-03 0.95    0    0    0
*****************************************************************************************
*GROUP 10 - User Specified Material Properties for Fuel and Clad                         *
*****************************************************************************************
**NGR
   10
*Card 10.1
** NMAT NDUM2 NDUM3 NDUM4 NDUM5 NDUM6 NDUM7 NDUM8 NDUM9 NDUM10 NDUM11 NDUM12 NDUM13 NDUM14
      2     0     0     0     0     0     0     0     0      0      0      0      0      0
*Card 10.2 and 10.3 are read together for each table
** Fuel Property Table
**  N    NNTDP      RCOLD              IMATAN
    1        1     7180.0               UZrH
** TPROP       CPF1   THCF
     300      0.276     18
** Cladding Property Table
**  N    NNTDP      RCOLD              IMATAN
    2        1     8030.0               SS304
** TPROP    CPF1   THCF
     100     0.5   16.2
*****************************************************************************************
*GROUP 11 - Core Power Distribution Information                                          *
*****************************************************************************************
**NGR
   11
*Card 11.1
** NQA  NAXP  MNXN    NQ NGPFF   NQR  NDM7  NDM8  NDM9 NDM10 NDM11 NDM12 NDM13 NDM14
     1     1    15     0     0     1     0     0     0     0     0     0     0     0
*Card 11.2
**          YQA
    0.00000E+00
*Card 11.3
**   I   NAXN
     1     15
*Card 11.4
**         Y      AXIALZ
  0.00000000  0.55278831
  0.02721429  0.56861377
  0.05442857  0.68996598
  0.08164286  0.81396568
  0.10885714  0.92248085
  0.13607143  1.01091673
  0.16328571  1.06431051
  0.19050000  1.15107140
  0.21771429  1.21641208
  0.24492857  1.24805385
  0.27214286  1.25027344
  0.29935714  1.22326535
  0.32657143  1.14315180
  0.35378571  1.03727954
  0.38100000  1.10745069
*Card 11.7
**          YQR
    0.00000E+00
*Card 11.8
**    FQR1      FQR2      FQR3      FQR4      FQR5      FQR6      FQR7      FQR8
 1.0000000
*****************************************************************************************
*GROUP 13 -  Boundary Condition Data                                                     *
*****************************************************************************************
**NGR
   13
*Card 13.1
```

```
** NBND   NKBD NFUN NGBD NDM5 NDM6 NDM7 NDM8 NDM9 NM10 NM11 NM12 NM13 NM14
      8      0    0    0    0    0    0    0    0    0    0    0    0    0
*Card 13.4
**Inlet b.c. ------------------------------------------------------------
** IBD1   IBD2 ISPC N1FN N2FN N3FN     BCVALUE1     BCVALUE2     BCVALUE3 INITGAS
      1      1    2    0    0    0  0.00000E+00 -0.30000E+02  0.00000E+00       1
      2      1    2    0    0    0  0.00000E+00 -0.30000E+02  0.00000E+00       1
      3      1    2    0    0    0  0.00000E+00 -0.30000E+02  0.00000E+00       1
      4      1    2    0    0    0  0.00000E+00 -0.30000E+02  0.00000E+00       1
**outlet b.c. -----------------------------------------------------------
      1     16    1    0    0    0  0.00000E+00  0.27130E+03  0.18000E+01       1
      2     16    1    0    0    0  0.00000E+00  0.27130E+03  0.18000E+01       1
      3     16    1    0    0    0  0.00000E+00  0.27130E+03  0.18000E+01       1
      4     16    1    0    0    0  0.00000E+00  0.27130E+03  0.18000E+01       1
*******************************************************************************************************
*GROUP 14 - Output Options
*******************************************************************************************************
**NGR
   14
*Card 14.4
**  N1  NOU1  NOU2  NOU3  NOU4  IPRP  IOPT  IITY   DNB IMASS IHEAT NDUM12 NDUM13 KRY
     7     0     0     0     0     0     0     0     0     0     0     0     0     0
*******************************************************************************************************
*GROUP 15 - Time Domain Data
*******************************************************************************************************
**NGR
   15
*Card 15.1
**     DTMIN        DTMAX         TEND        EDINT       DMPINT        RTWFP     MAXITS
  0.1000E-04  0.1000E+01  0.0000E+00  0.0000E+00  0.0000E+00  0.1000E+04      10000
*******************************************************************************************************
*GROUP 17 - Channel/Rod Maps for HDF5 and VTK files
*******************************************************************************************************
**NGR
   17
*Card 17.1 - HDF5_NAME VTK_NAME
TRIGA_Pin11471_Unblocked.hdf5 TRIGA_Pin11471_Unblocked.vtk
*Card 17.2 - Rod Map Dimensions
**TOTRODSROW TOTRODSCOL
           1          1
*Card 17.3 - Channel Map Dimensions
**TOTCHANSROW TOTCHANSCOL
           2          2
*Card 17.4 - Rod Map
  1
*Card 17.4 - Channel Map
  1  1
  1  1
*******************************************************************************************************
*GROUP 18 - Convergence Criteria for Steady State Solve
*******************************************************************************************************
**NGR
   18
*Card 18.1
**Global Energy Balance Criteria (%)
  0.010000
*Card 18.2
**Global Mass Balance Criteria (%)
  0.010000
*Card 18.3
**Fluid Energy Storage Criteria (%)
  0.500000
*Card 18.4
**Solid Energy Storage Criteria (%)
  0.500000
*Card 18.5
**Mass Storage Criteria (%)
  0.500000
```

APPENDIX C

This appendix contains more detail and the order of bugs and errors that were encountered during the use of CTF, specifically during the PWR analysis.

Due to limitations with running CTF in parallel and the server size available for use, the largest model that could be run was a full scale 8^{th} core model. CTF requires one processor core per assembly in order to run in parallel, therefore, an 8^{th} core model requires 31 processor cores in order to run. In this model, each assembly was modeled in full 17x17 detail in order to see exactly what happens in the core. Since the RELAP5-3D model already used a very coarse lumping method, the full detail with CTF is necessary in order to validate the RELAP5-3D model and ensure that all in-core phenomena are being accounted for.

One of the limitations that was found with CTF was that the transient features of CTF are still in their infancy. Having tested CTF with multiple transient scenarios, errors continued to interrupt the simulations. However, testing of the transient features resulted in significant improvements to CTF as a developing code. Some errors were misprints within the user manual that instructed incorrect set up of the input decks. Other issues were related to bugs in the source code.

First, two bugs were found within the preprocessor tool which is useful for automatically generating the CTF input decks without creating all the geometry manually. One of the bugs that was found within the preprocessor did not affect the creation of the CTF input deck as the preprocessor would complete successfully. However, it created a bugged CTF input deck by not including special notation on

specific lines of the CTF input deck to denote transient parameters such as step size, simulation time, etc. Once this bug was addressed, it was discovered that the preprocessor was not originally designed to create transient input decks but was currently in the process of being modified to accommodate transient parameters. This resulted in every transient input deck being cross-checked and edited manually to ensure that all necessary parameters were present for CTF, particularly in card 11 (power data) and card 15 (transient parameters). This became quite cumbersome considering parallel computing was being used at the same time and a CTF input deck is generated for each assembly in the simulation. With this new information, a second bug was found in which card 11.5 was not being written into the CTF input decks at all. This bug was addressed and fixed as well.

Once the issues with the preprocessor were realized, corrected CTF input decks were created by manually cross-checking the CTF input decks to verify that they were correct before running CTF. Once a transient simulation had finally completed with CTF, it was realized that there were no visualization files (vtk) being generated, therefore the data was only available in a text file and visualization software was not able to be used to see results. This resulted in manually parsing the output files for the desirable data and plotting it manually. The lack of visualization files was fixed in revisions to CTF, resulting in the production of visualization files for transient simulations. This welcomed new formatting to the CTF input decks by including new parameters in the CTF input deck that must be included in all CTF input decks in order

for the vtk files to be produced. However, these edits had to be made manually as the preprocessor did not reflect these changes.

After these changes were made, it became difficult to run the transient simulations that were needed. Simple models that were expected to run within a few minutes were running for more than 48 hours before they were aborted. This brought upon new issues to look into.

A few additional bugs were finally discovered. The first one caused system arrays to be allocated multiple times in the vtk writing step, which would happen at every EDIT interval (interval at which a current simulation status output is generated). While this would cause a crash on some computer systems, on the computer system being used it caused CTF to stall and never finished running until the simulation was terminated.

The second bug that was found that also created issues was with the preprocessor. This time, if in a transient simulation the power changed over the course of the simulation, the preprocessor was supposed to generate a forcing function and write it into CTF input deck. However, this power forcing function was not created and resulted in a steady power for the CTF simulation. This was an issue because to model the scenario of interest, a decay power scheme must be modeled for the reactor core.

While looking into these bugs, another, unrelated, set back of CTF running transients was discovered. In order to run a similar simulation that was run using RELAP5-3D, steady-state would have to be reached at normal operating conditions before the accident scenario is introduced. This was the realization of the first weakness

of CTF transient simulations. Since it is impossible to change the mass flow rates in CTF over time, this would require running a steady-state simulation with CTF, then running a transient simulation picking up where the steady-state simulation left off. While this was a feature that is expected to be added to CTF and working at some point, at the current time, it is not functional.

Once these bugs were addressed, CTF was used to run the transient simulations again, and this time, they finished and yielded output files. However, the simulations were designed to run for a 15 second transient and would end at approximately 14.9998 seconds. This caused CTF to not create a visualization file for the end of the simulation at 15 seconds. This also caused some of the simulation information such as simulation run time to be missing in the output files. This issue was investigated and it was finally discovered that there was an issue with the parallel algorithm. One of the time step controls was not properly distributed between various domains of the solution, so one processor would fall behind the others in the transient simulation. This meant that the processors that were ahead would eventually get to a point where they should produce a vtk file, but the lagging processor would not be ready, therefore, the simulation would cease and finish incorrectly.

Once this issue was addressed, these simulations were run again with the updated CTF code. Majority of the testing simulations were running correctly, however, when more complicated simulations were run using varying inlet mass flow rates and mass fluxes for different assemblies, the vtk files created were missing vector data. While this issue was being investigated, it appeared that CTF was writing the vtk file incorrectly.

Upon further investigation, it became questionable as to the best way to model varying inlet mass flow rates or mass fluxes. As stated earlier, in parallel simulation, CTF creates an input deck for each assembly of the simulation. These assemblies are designed to slightly overlap each other, therefore, the sub-channels at the edge of an assembly might be shared in an adjacent assembly input deck. When trying to specify a different mass flux for each assembly, CTF can use a total mass flux for an assembly specified in the input deck and then uses geometry input to compute mass flow rate for each individual sub-channel. This would function for a serial simulation, however, in a parallel simulation, this causes some sub-channels to have two different calculated mass flow rates in two adjacent assembly CTF input decks of the simulation. This does not seem to trigger an error with CTF, however, creates issues in the output files and might even yield false data.